

NASA Technical Paper 1516

Wind-Tunnel/Flight Correlation Study  
of Aerodynamic Characteristics  
of a Large Flexible Supersonic  
Cruise Airplane (XB-70-1)

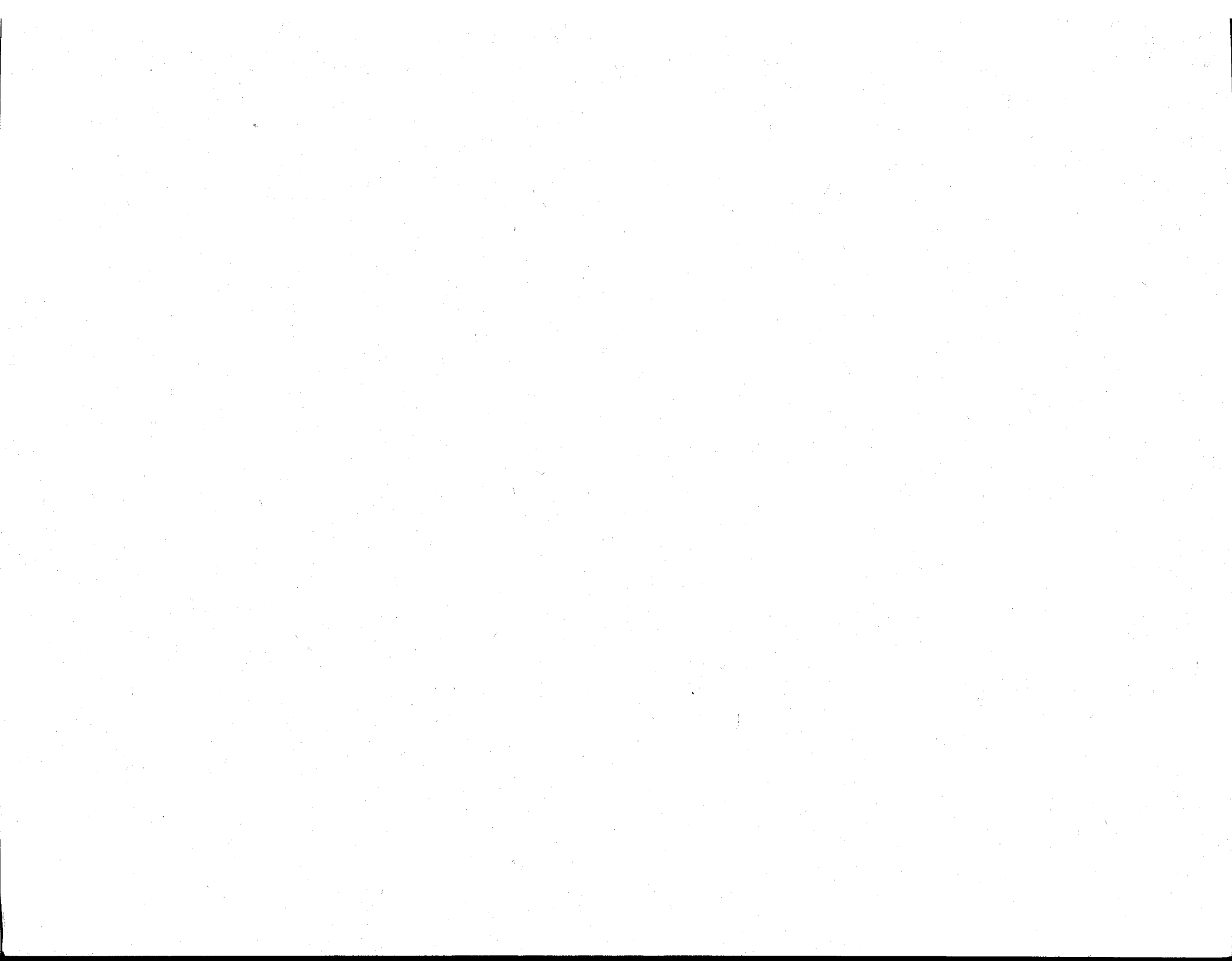
III - A Comparison Between Characteristics  
Predicted From Wind-Tunnel Measurements  
and Those Measured in Flight

Henry H. Arnaiz, John B. Peterson, Jr.,  
and James C. Daugherty

MARCH 1980

CASE FILE  
COPY

**NASA**



Wind-Tunnel/Flight Correlation Study  
of Aerodynamic Characteristics  
of a Large Flexible Supersonic  
Cruise Airplane (XB-70-1)

III - A Comparison Between Characteristics  
Predicted From Wind-Tunnel Measurements  
and Those Measured in Flight

Henry H. Arnaiz

*Dryden Flight Research Center, Edwards, California*

John B. Peterson, Jr.

*Langley Research Center, Hampton, Virginia*

James C. Daugherty

*Ames Research Center, Moffett Field, California*



National Aeronautics  
and Space Administration

**Scientific and Technical  
Information Office**



## SUMMARY

A program was undertaken by the NASA to evaluate the accuracy of a method for predicting the aerodynamic characteristics of large supersonic cruise airplanes. This program compared predicted and flight-measured lift, drag, angle of attack, and control surface deflection for the XB-70-1 airplane for 14 flight conditions with a Mach number range from 0.76 to 2.56.

The predictions were derived from the wind-tunnel test data of a 0.03-scale model of the XB-70-1 airplane fabricated to represent the aeroelastically deformed shape at a 2.5 Mach number cruise condition. Corrections for shape variations at the other Mach numbers were included in the prediction.

For most cases, differences between predicted and measured values were within the accuracy of the comparison. However, there were significant differences at transonic Mach numbers. At a Mach number of 1.06 differences were as large as 27 percent in the drag coefficients and  $12^\circ$  in the elevator deflections. A brief analysis indicated that a significant number of the differences observed between predicted and measured drag coefficients were due to the incorrect prediction of the control surface deflection required to trim the airplane.

## INTRODUCTION

An important factor in the design and development of an airplane is the accurate prediction of aerodynamic characteristics from wind-tunnel tests of small-scale models. For large supersonic cruise airplanes, like a supersonic transport, accurate prediction is extremely important since small errors may have severe economic penalties if the airplane does not operate as designed. Determining the accuracy of a prediction method, however, is a problem. One reason is that there is a lack of accurate in-flight measurements of aerodynamic characteristics to compare with. For some cases where measurements were obtained, comparisons have been made (refs. 1 to 12). Unfortunately most of these have been at subsonic and transonic Mach numbers. In other cases, wind-tunnel models that did not accurately correspond to the flight test airplane were used, or all of the extrapolation items that are necessary for a prediction were not included.

During the flight research program of the XB-70-1 airplane conducted by the National Aeronautics and Space Administration, accurate in-flight measurements of the aerodynamic characteristics were made (refs. 13 to 15). Because the size, speed, and design were comparable in many respects to a supersonic transport, NASA used this opportunity to evaluate the method of predicting aerodynamic characteristics for large supersonic cruise airplanes. The flight-measured aerodynamic characteristics were compared with those predicted from wind-tunnel tests for a selected number of flight conditions covering a large Mach number

range. This was a cooperative effort by three NASA Research Centers (Ames, Dryden, and Langley) and the airplane manufacturer, on contract. The major elements of this program are described below:

(1) Fourteen flight conditions were selected for which aerodynamic characteristics could be compared. These conditions were selected from nearly 100 measured and analyzed flight conditions obtained by the Dryden Flight Research Center (ref. 15). The conditions were distributed over a Mach number range from 0.76 to 2.56 with a concentration at the transonic Mach numbers and near a Mach number of 2.50.

Because at each flight condition the airplane had a unique configuration, the 14 flight conditions are referred to herein as comparison points in order to avoid any confusion resulting from differences in airplane configuration at similar flight conditions. Notation for the comparison points established in reference 16 was adopted in this investigation.

(2) The deformed shape of the airplane in flight was calculated for the comparison points by the airplane manufacturer so the effect of structural flexibility on the aerodynamic characteristics could be incorporated into the prediction. These shapes along with flexibility information are presented in reference 16.

(3) A rigid, 0.03-scale wind-tunnel model was built for this program by the airplane manufacturer. It was specifically designed and fabricated to represent the steady state flexible shape of the XB-70-1 airplane at one of the comparison points - P8 (refs. 16 and 17). The Mach number for this point was 2.53, and the altitude was 19,187 m (62,950 ft). Model design and fabrication are described in references 16 and 17. Information required to extrapolate the small-scale model wind-tunnel data to specified full-scale flight conditions is provided in reference 16.

(4) The model was tested in the Unitary Plan Wind Tunnel at the Ames Research Center. Reference 17 presents the data and describes the techniques and procedures used for the tests.

(5) The prediction consisted of the analytical work of adjusting and extrapolating the wind-tunnel test data to the flight conditions and airplane configurations for each of the 14 comparison points. The Langley Research Center performed this part of the program, as reported in reference 18.

(6) The comparison was then made between the measured and predicted aerodynamic characteristics - lift, drag, angle of attack, and longitudinal control surface deflection. This report presents this comparison along with a brief description of the 14 comparison points, the wind-tunnel tests, and the prediction process.

SYMBOLS

$C_D$	drag coefficient
$C_L$	lift coefficient
$C_M$	pitching moment coefficient
cg	center of gravity
g	acceleration due to gravity, m/sec <sup>2</sup> (ft/sec <sup>2</sup> )
M	Mach number
MAC	mean aerodynamic chord, m (ft)
P1 to P10	flight test point identification number
$q_\infty$	free-stream dynamic pressure, N/m <sup>2</sup> (lb/ft <sup>2</sup> )
$R_{MAC}$	Reynolds number based on MAC
$t_\infty$	free-stream static temperature, K (°R)
x	distance along the MAC, m (ft)
$\alpha$	angle of attack, deg
$\Delta$	incremental value
$\delta_{byp}$	inlet bypass door deflection, deg
$\delta_c$	canard deflection (positive leading edge up), deg
$\delta_e$	elevator deflection (positive trailing edge down), deg
$\delta_t$	wingtip deflection (positive down), deg
Subscripts:	
flex	condition due to flexibility
meas	measured
pred	predicted
rigid	condition due to rigid structure
$\infty$	free stream

## AIRPLANE

The XB-70-1 airplane (figs. 1 and 2) was a large, delta-winged supersonic cruise aircraft designed for sustained flight at Mach numbers up to 3 at an altitude of 21,340 meters (70,000 feet). The airplane had a gross takeoff mass in excess of 226,800 kilograms (equivalent to a weight of 500,000 pounds) and an empty mass of approximately 124,740 kilograms (equivalent to a weight of 275,000 pounds). The pertinent physical characteristics of the airplane are given in table 1.

The airplane design incorporated a thin wing with a  $65.6^\circ$  leading-edge sweep and downward-folding wingtips for increased stability at high speeds. The nominal wingtip folding schedule and operating limits are shown in figure 3.

The fuselage had a long, slender, cylindrical section forward and above the wing plane. The nose ramp in front of the cockpit had two positions: it was lowered for visibility at low speeds, and it could be raised for wave drag reduction at supersonic speeds.

There was a movable low-aspect-ratio canard directly behind the cockpit. The canard had a flap that was deflected during takeoff and landing. In the normal flight configuration, the flap was not deflected and canard position was geared to the elevons for pitch control.

The elevator-to-canard gearing curve was designed as shown in figure 4. However, the airplane control system caused small but significant shifts to the linear relationship (ref. 16). These shifts, as discussed in reference 18, were included in the prediction.

The elevons were split into six spanwise segments on each wing semispan to prevent binding from wing bending. When the wingtips were deflected, the two outermost segments were faired (zero deflection) and became part of the folded wingtip. Twin, movable vertical stabilizers with inclined hinge lines provided directional stability and control. Figure 5 shows the XB-70-1 control surfaces and their deflection limits.

The propulsion system, which consisted of the inlet and engines, occupied most of the lower rear fuselage as shown in figure 6. The inlets were of the two-dimensional mixed-compression type and were designed to operate efficiently at high supersonic speeds. Each inlet was equipped with fixed vertical ramps in front of the cowl lip and variable ramps in the region of the throat to control throat area. There were six bypass doors for each inlet on top of the wing just in front of the engine face between the vertical tails (fig. 7). The inlet ramps and bypass doors were used to optimize the performance of the inlet throughout the speed range.

The boundary layer about the inlet throat was bled off to reduce shock-induced boundary layer separation. A two-dimensional ram scoop bled the boundary layer from the ceiling of the duct; this air was ducted through and dumped over the upper surface of the wing through a diverter (fig. 7). Boundary layer air from the side walls and floor of the inlet near the throat was removed through 8-percent porosity bleed panels. Part of this air was dumped underneath

the inlet through louvers and a bleed dump fairing with an exit like an aft-facing step (figs. 6 and 7). The rest of the bleed was ducted to the base region of the airplane (figs. 7 and 8), increasing the pressure in this region and thereby reducing base drag.

The inlets supplied air to six YJ93-GE-3 afterburning turbojet engines, which were mounted side by side, three engines per inlet, in the rear section of the nacelle. The engines were rated at 133,500 newtons (30,000 pounds) sea level static thrust and had a compressor airflow capability of 120 kilograms per second (264 pounds per second) and an 8.7-to-1 pressure ratio. Each engine was equipped with an 11-stage axial-flow compressor with variable stators, an annular combustion system, a two-stage air-cooled turbine, and mechanically linked variable-area primary and secondary exhaust nozzles.

The engines exhausted into the airplane's large base region (fig. 8). This region was divided into compartments that housed the engines individually and was somewhat unusual in that the upper and lower surfaces of the fuselage terminated at different fuselage stations, causing the engine nozzles to overhang the lower fuselage surface. The base region did not have an aft-facing bulkhead type of surface; the most rearward surface of this type was the engine's rear firewall, which was approximately 4.57 meters (15 feet) in front of the engine's exit plane.

#### COMPARISON POINTS

Table 2 summarizes the flight conditions and the measured aerodynamic characteristics and configuration of the airplane at each of the comparison points. The values were taken directly from references 15 and 16 with the exception of  $\alpha_{meas}$  values which were corrected for fuselage bending.

Figure 9 shows the comparison points with respect to the flight envelope of the airplane (altitude versus Mach number) and the climb profile for a Mach 3.0 cruise flight. As can be seen, only two of the comparison points were at subsonic speeds (Mach numbers of 0.76 and 0.93). Comparison points at Mach numbers of 0.93, 1.06, 1.15, 1.17, and 1.18 were chosen to investigate transonic Mach numbers, which have usually been a problem for wind-tunnel and theoretical simulations of flow fields, and to a lesser degree in flight measurements. Supersonic comparison points were chosen at Mach numbers of approximately 1.6, 2.1, and 2.5.

In order to investigate drag polars, four comparison points were chosen at load factors for other than lg flight at the approximate Mach numbers of 1.18 (P3L and P3H) and 2.50 (P8L and P8H). These points can be easily identified in figure 10, which shows the region of lg flight. These high and low lift coefficients were generated by increasing and decreasing the load factor of the airplane through a roller coaster maneuver described in reference 15.

## WIND-TUNNEL TESTS

Accurate and comprehensive wind-tunnel test data are essential to the prediction of aircraft characteristics. For this study, wind-tunnel investigations were done in the manner of validation tests conducted to determine aerodynamic performance parameters during aircraft design and development. Necessary corrections were meticulously determined and applied to the test data. At the same time, only accepted procedures or techniques were used in the wind-tunnel tests.

### Model Description

A 0.03-scale, static force model of the XB-70-1 airplane was constructed by the airplane manufacturer to be used in the test program. The rigid model was designed and fabricated to be representative of the steady state flexible shape estimated to exist at the speed-power-stabilized flight test condition at a Mach number of 2.53 (data point 72 of ref. 15 - same as point P8 of ref. 16).

Schematic drawings are presented in figure 11, and installation of the model in the wind tunnel is shown in figure 12. The model was sting mounted from the rear. Model forces and moments were measured by means of a 6-component internal strain gage balance mounted in the model. Pressures on the model base and in the balance cavity and internal flow ducts were measured with a pressure-sampling valve-drive-transducer combination mounted in the forebody of the model.

The quality of the model was comparable to that normally used for performance-validation wind-tunnel tests. The model was designed to be very rigid, minimizing flexibility effects on the final test results. During both fabrication and preparation for testing, extreme care was taken in regard to geometrical tolerances, surface finish, and overall workmanship.

### Test Description

The tests were conducted in the 11- by 11-foot transonic and the 9- by 7-foot supersonic test sections of the Ames Research Center Unitary Plan Wind Tunnel. Test Mach numbers ranged from 0.60 to 2.53. The model was not tested, however, between the transonic Mach numbers of 0.95 and 1.2 because of possible wall interference and shock wave reflection. The unit Reynolds number was  $13.12 \times 10^6$  per meter ( $4 \times 10^6$  per foot). The basic rigid model configuration and shape represent those of the XB-70-1 airplane at P8 in table 2, neglecting the trim and control surfaces (canards, elevons, and rudders), which were set to zero deflection. During the tests, however, all trim and control surfaces, including the wingtips, were deflected to cover the range of deflection angles encompassed during the flight tests of the airplane. Angle of attack ranged from  $-5^\circ$  to  $10^\circ$ . Angle of sideslip varied from  $-5^\circ$  to  $5^\circ$ . During the tests certain component effects such as inlet mass flow variations, boundary layer trip size, and so forth, were investigated to permit interpretation and extrapolation of the test results to flight test conditions.

## Corrections to Wind-Tunnel Test Data

Corrections were made to all of the wind-tunnel data; the following briefly describes them.

Tunnel stream angle.- The angle of attack was corrected for the tunnel stream angles. Corrections varied from  $0.1^\circ$  at 0.60 Mach number to  $-0.05^\circ$  at 2.53 Mach number.

Model support.- Corrections to both the angle of attack and angle of sideslip were made for the bending of the model support, sting, and balance due to aerodynamic and weight loads.

Model base drag.- The drag data were adjusted to correspond to a condition of free-stream static pressure in the balance cavity and on the model base. The base drag on the inlet bleed dump fairing was adjusted in a similar manner.

Wind-tunnel buoyancy.- Corrections for effects from clear-tunnel static pressure variations along the tunnel test section, resulting from the presence of the model and support apparatus, were applied to data obtained in the 9- by 7-foot test section.

Internal flow drag.- The internal drag of the inlet ducts was subtracted from the measured drag. This correction was obtained by measuring the losses in momentum and pressure forces as referred to the free-stream pressure for the air flowing through each duct.

Alinement of balance cavity.- Data were corrected for a misalignment of  $0.03^\circ$  between the centerline of the balance cavity and the reference plane.

## PREDICTION PROCEDURE

The analysis for the prediction was performed by the Langley Research Center and is presented in detail in reference 18. The prediction process first generated basic aerodynamic characteristics from the wind-tunnel data at the Mach numbers that corresponded to the comparison points. Next these characteristics were adjusted for items which were not properly simulated or represented on the wind-tunnel model. The last step was to predict the coefficient of drag, angle of attack, and control surface deflections for the 14 comparison points at the flight-measured lift coefficient and aircraft center of gravity location.

The following briefly describes and presents the results of each of the basic steps and procedures that were used in the prediction.

### Generation of Basic Aerodynamic Characteristics

Coefficients for lift, drag, and pitching moment,  $C_L$ ,  $C_D$ , and  $C_M$ , respectively, were determined from the wind-tunnel data at the Mach numbers that

corresponded to 13 of the 14 comparison points. These coefficients were derived by linearly interpolating the wind-tunnel data over a range of angles of attack and control surface deflections that encompassed those measured in flight. However, this technique could not be used for the P10 comparison point since wind-tunnel data were not available near a Mach number of 1.06. Instead, data at Mach numbers of 0.80, 0.95, 1.20, and 1.4, along with experience and knowledge of how the aerodynamic characteristics behave through the transonic region, were used to establish the required aerodynamic characteristics.

#### Adjustments to the Basic Wind-Tunnel Data

The small adjustments required to make the basic wind-tunnel data represent the aircraft configuration are as follows:

Wingtip angle.- Deflections of the wingtips were measured for each of the comparison points. The angles were found to be slightly different from the nominal wind-tunnel test deflection angles of  $0^{\circ}$ ,  $25^{\circ}$ , and  $65^{\circ}$ . Corrections were determined from wind-tunnel tests made with the wingtips deflected at angles slightly different from the nominal deflections.

Rudder deflection.- For the small deflections in rudder that were measured in flight, the wind-tunnel results showed that the changes in the lift, drag, and pitching moment coefficients were insignificant.

Shaker vane.- Small shaker vanes were located on each side of the XB-70-1 fuselage ahead of the canard for all of the comparison points except P7 and P10. The model was tested in the wind tunnel, with and without the vane, to determine the incremental forces generated by the vane.

Canopy position.- A two-position ramp existed ahead of the canopy of the XB-70-1. When the ramp was up (the high speed position) it faired the body lines so that wave drag was reduced at supersonic speeds. In the down position (used at low speeds) it allowed the crew greater visibility. The ramp was in the down position for all comparison points except P8, P8L, and P8H.

Spillage drag.- A reference inlet capture mass flow ratio, which represents the nominal mass flow ratio that was measured in flight for the XB-70-1 airplane, is shown in figure 13 as a function of Mach number. The inlet mass flow ratio of the model was maintained very close to the reference schedule during the wind-tunnel tests by choosing the proper exit nozzle area. Small corrections to the data for both the model and the airplane were made for conditions where the inlet mass flow ratio was different from the reference. The corrections were determined using wind-tunnel test data where the mass flow ratio was varied at each Mach number by using different metering nozzles in the inlet exit ducts. These corrections were made for Mach numbers of up to 2.0; above that Mach number the inlet began to operate in a mixed-compression mode. In this mode, the inlet mass flow ratio is determined mainly by the geometry of the inlet.

Boundary layer trip drag.- Boundary layer trips, consisting of narrow strips of glass beads, were used to establish the turbulent flow on the wind-

tunnel model. Several different sizes of glass beads were tested to determine the variation of the drag coefficient with bead size (ref. 18). This test indicated that the bead size used in obtaining the majority of the wind-tunnel data was sufficiently large, not only to trip the boundary layer, but also to produce an increment of drag. This increment was subtracted from the wind-tunnel data.

Model afterbody.- An afterbody that allowed greater clearance around the support sting was used in the tests for the Mach number range of 0.6 to 1.4. The effect of this larger afterbody was determined by testing the normal afterbody at low angles of attack at the same Mach numbers.

Even though the normal model afterbody conformed closely to the XB-70-1 airplane, there was a slight difference in the closure at the end of the fuselage. The difference in wave drag was calculated with the Langley Research Center wave drag programs and incorporated into the prediction.

Skin-friction drag.- Corrections for skin-friction drag were necessary because of significant differences in the Reynolds number of the airplane in flight and of the wind-tunnel model. Skin-friction drag was calculated for the model and the XB-70-1 airplane for the flight conditions of each comparison point using flat-plate skin-friction drag coefficients adjusted with shape factors for the various components. The shape factors (from ref. 19) included the effects of taper ratio and the increase in dynamic pressure from shock waves impinging on surfaces, such as the inlet duct sides, at supersonic speeds. The wall temperature on both the airplane and the model was assumed adiabatic. Though there is some excursion of wall temperature from adiabatic in flight, calculations based on measured flight data indicated the effect to be minimal (ref. 20).

Propulsion system.- Corrections in  $C_D$  and  $C_M$  attributed to the bypass doors and the boundary layer bleed dumps were incorporated in the prediction. The drag of the bypass doors was calculated from the theoretical pressure on the surface of the front set of doors, which were open only at supersonic speeds. The drag of the boundary layer bleed dump fairing underneath the inlet was calculated with the Langley wave drag computer program.

The interference drag, caused by the airflows from the inlet bleed and those from the bypass and diverter exits interacting with the surrounding surfaces of the airplane, was estimated in reference 16 from data obtained from flush and protruding exhaust nozzles and incorporated in the prediction.

Flexibility.- The airplane manufacturer (ref. 16) provided information to adjust rigid-model wind-tunnel aerodynamic characteristics for the effects of the bending and twisting of the airplane structure in flight. The camber shape for the entire airplane was provided at each comparison point.

Lift, drag, and pitching moment at the angle of attack of each comparison point were calculated for the airplane and model shapes. The differences in aerodynamic characteristics between the airplane and model shape were added to the wind-tunnel data (see ref. 18).

No attempt was made to correct comparison point P10 since linearized supersonic theory does not treat the transonic flow phenomena adequately.

Small adjustments to the wind-tunnel data for  $C_L$ ,  $C_D$ , and  $C_M$  were made for P8. This was necessary because the shape of the airplane was recalculated after the wind-tunnel model was built and tested and was found to be slightly different from that originally calculated.

Roughness, protuberance, and air leakage drag.- The airplane was closely examined for roughnesses such as holes, screw and rivet heads, steps, patches, and so forth. In total, 852 items were located and measured. The drag was determined by the techniques described in reference 18.

The drag of protuberances on the XB-70-1 airplane such as lights, test instrumentation, probes, vents, and so forth, is presented in reference 16. The technique used for calculating the drag is presented in reference 21.

Airflow rates through gaps in items like the landing gear doors were not measured in flight and, therefore, had to be estimated. The calculations were based on the change in momentum of air leakage (see ref. 16).

Base drag.- No attempt was made to estimate the base drag on the airplane for this study because of the expense of a jet-powered model. Therefore, in order to eliminate this possible source of error from the comparison, the flight-measured base drag values were used in the prediction.

#### Prediction Results and Summary

Sets of curves of the predicted aerodynamic characteristics for the XB-70-1 airplane are shown for the 14 comparison points in figures 14(a) to 14(j). These curves include the adjustments and corrections made to the basic wind-tunnel data. In addition, flexible-to-rigid ratios were applied to the basic wind-tunnel-derived aerodynamic characteristics to incorporate changes in the aircraft shape at other angles of attack and control deflection other than those originally determined. The ratios are presented in reference 16 and correct both lift and moment coefficients in terms of changes in  $\alpha$  and elevon and canard deflections. The ratios used to determine  $C_L$  are

$$\frac{\left(\frac{\Delta C_L}{\Delta \alpha}\right)_{\text{flex}}}{\left(\frac{\Delta C_L}{\Delta \alpha}\right)_{\text{rigid}}}, \quad \frac{\left(\frac{\Delta C_L}{\Delta \delta_e}\right)_{\text{flex}}}{\left(\frac{\Delta C_L}{\Delta \delta_e}\right)_{\text{rigid}}}, \quad \text{and} \quad \frac{\left(\frac{\Delta C_L}{\Delta \delta_c}\right)_{\text{flex}}}{\left(\frac{\Delta C_L}{\Delta \delta_c}\right)_{\text{rigid}}}$$

The ratios used to determine  $C_M$  are

$$\frac{\left(\frac{\Delta C_M}{\Delta \alpha}\right)_{\text{flex}}}{\left(\frac{\Delta C_M}{\Delta \alpha}\right)_{\text{rigid}}}, \quad \frac{\left(\frac{\Delta C_M}{\Delta \delta_e}\right)_{\text{flex}}}{\left(\frac{\Delta C_M}{\Delta \delta_e}\right)_{\text{rigid}}}, \quad \text{and} \quad \frac{\left(\frac{\Delta C_M}{\Delta \delta_c}\right)_{\text{flex}}}{\left(\frac{\Delta C_M}{\Delta \delta_c}\right)_{\text{rigid}}}$$

Although flexible-to-rigid ratios were not required for  $C_D$ , the drag polars of figures 14(a) to 14(j) do contain drag changes resulting from flexible-to-rigid ratio changes in  $C_L$  and  $C_M$ .

From figures 14(a) to 14(j), predicted  $C_D$ ,  $\alpha$ ,  $\delta_e$ , and  $\delta_c$  were obtained by using the following procedure.

The flight-measured  $C_L$  and center of gravity (cg), referenced to the mean aerodynamic chord (MAC), were used to determine  $C_{M,meas}$  referenced to the 25 percent MAC location with the equation

$$C_{M,meas} = -C_{L,meas} (cg - 0.25)$$

This equation was derived from the general expression shown below, which converts any moment along the MAC to the 25 percent MAC location.

$$C_{M,x/MAC} = C_M + C_L(x/MAC - 0.25)$$

Values for  $\delta_{e,pred}$  and  $\delta_{c,pred}$  can be obtained by using the  $C_{M,pred}$  plot in figure 14 to trim the airplane to the  $C_{M,meas}$  at the  $C_{L,meas}$ . Similarly, curves were used to predict drag values and angles of attack at  $C_{L,meas}$  using the  $\alpha_{pred}$  and  $C_{D,pred}$  plots in figure 14.

Figures 15 to 17 summarize the contributions from the basic wind-tunnel data and the adjustments that were used to predict  $C_L$ ,  $C_D$ , and  $C_M$ . The largest adjustments in  $C_{D,pred}$  (fig. 16) were for trim, skin-friction drag, and base drag. It should be noted that the adjustments for flexibility were relatively small and resulted mostly from a change in drag due to lift at a constant angle of attack.

Figure 17 shows the size of the elements contributing to making up the moment coefficient required to trim the predicted data to the flight-measured center of gravity. The significant adjustments were for the elevator and canard deflections, and to a lesser degree, for flexibility.

Table 3 shows the predicted values for each of the 14 comparison points. In general, these values should be quite accurate, since state-of-the-art methods were used in the prediction process, eliminating many of the areas where errors might have resulted. Some of the more important factors contributing to the accuracy of the prediction are summarized below:

(1) Specific flight conditions and airplane configurations were evaluated, rather than a nominal condition of a representative configuration.

(2) The wind-tunnel model geometry was more representative of the actual airplane geometry than is usually the case.

(3) Adjustments were made to the wind-tunnel data for the actual shape of the airplane in flight as determined from an extensive flexibility study (both analytical and experimental) of the actual aircraft structure.

(4) Drag increments from measured skin roughness, known protuberances, and estimated air leakage were included in the prediction.

(5) Propulsion system forces charged to the airplane were determined and incorporated into the prediction.

(6) Base drag, which was a significant percentage of the airplane drag at some flight conditions, was measured in flight and incorporated into the prediction, rather than attempting to predict it.

(7) A concentrated effort was made throughout this correlation study to keep human errors to a minimum. This was a difficult task and required considerable cross checking of the numerous calculations. If strict attention were not applied to this effort, significant discrepancies could have resulted and would have been difficult to detect in the final results.

This prediction provided an excellent opportunity to examine the size of each contributing element to the final predicted values of  $C_L$ ,  $C_D$ , and  $C_M$ . This information can be quite useful in the design of a supersonic cruise aircraft, since many of these elements are only estimated and never verified, as was done in this prediction.

#### COMPARISON BETWEEN PREDICTED AND FLIGHT-MEASURED CHARACTERISTICS

The predicted and measured values for  $\alpha$ ,  $C_D$ , and  $\delta_e$  for flight-measured  $C_L$  and  $C_M$  are compared in figure 18. Included in this figure are the flight-measured drag polars and the  $C_L$  versus  $\alpha$  relationships, which were established in reference 15. Canard deflections are not included, since the gearing between  $\delta_c$  and  $\delta_e$  results in differences between the predicted and measured values of  $\delta_c$  that are 15 percent of the differences between  $\delta_{e,pred}$  and  $\delta_{e,meas}$ .

A summary plot showing the differences observed between measured and predicted  $C_D$ ,  $\alpha$ , and  $\delta_e$  is presented as a function of  $M_\infty$  for the 14 comparison points in figure 19. As can be seen from this figure and figure 18, agreement between predicted and measured characteristics ranged from good to poor for the three parameters evaluated. Only at one Mach number ( $M_\infty = 1.06$ ) were significant differences seen for all three parameters. However, large differences were expected in this Mach number region for two reasons: First, the acceleration rate of the airplane was much lower than expected in flight along with exceptionally large elevator deflections (ref. 22); second, neither wind-tunnel data nor flexibility adjustments were available for the prediction.

## Coefficient of Drag

The combined accuracy (root mean square value) of the flight test measurements, the wind-tunnel test data, and the prediction was estimated to be approximately 7 percent (refs. 15 and 23). As can be seen in figure 19, approximately half of the data points fell inside a  $\pm 7$  percent  $\Delta C_D$  band. The largest differences were seen in the transonic Mach number regime ( $0.9 < M_\infty < 1.2$ ), with 27 percent at  $M_\infty = 1.06$  being the largest difference observed. An incorrect prediction of this magnitude can be critical if an airplane's margin of excess thrust is small in this Mach number region. On one occasion the XB-70-1 airplane could not accelerate past a Mach number of 1.06 because of the loss in engine thrust caused by an ambient temperature of  $13^\circ \text{C}$  ( $23^\circ \text{F}$ ) above standard day temperature. Only after the weight of the airplane had been reduced significantly by the large quantity of fuel consumed at maximum power could the airplane accelerate supersonically.

Other data points outside the  $\pm 7$  percent accuracy band, at Mach numbers of 1.18 and near 2.1 and 2.5, appear to depend on the lift coefficient. There was a tendency for the differences to increase with increasing  $C_L$ , as seen in figures 18(d), 18(f), and 18(g).

## Angle of Attack

Differences in  $\alpha$  that were larger than the expected combined accuracy of the flight-measured data, the wind-tunnel test data, and the prediction (approximately  $0.3^\circ$ ) were seen at Mach numbers of 0.93, 1.06, and near 2.5. The most significant point was near a Mach number of 2.5. There was a shift of approximately  $0.5^\circ$  in the  $C_L$  versus  $\alpha$  curve (fig. 18(g)) at this Mach number. The differences between predicted and measured  $\alpha$  varied from  $0.4^\circ$  to  $0.8^\circ$ , and are important for two reasons: (1) A large difference in  $\alpha$  occurred even though a concentrated effort was made to make the best prediction possible at this Mach number, and (2) differences in  $\alpha$  can lead to significant errors in determining  $C_D$  from the axial force coefficient and the normal force coefficient in the wind tunnel or from normal and longitudinal accelerations in flight (as shown in refs. 15 and 23).

## Longitudinal Control Surface Deflections

The differences between the predicted and measured elevator deflections were at least  $2^\circ$  for all points, with the exception of the comparison points near Mach numbers of 0.76, 1.6, and 2.5, as shown in figure 19. The maximum difference observed,  $12^\circ$ , was at a Mach number of 1.06. This magnitude of deflection was approximately 30 percent of the control authority of the airplane.

Part of the differences in the drag coefficients of the transonic Mach numbers was due to the incorrect estimation of trim drag. The pitching moment was not accurately predicted from the wind-tunnel data in this Mach number

regime. When drag was predicted using flight-measured values for  $\delta_e$  and  $\delta_c$ , instead of those deflections required to trim the airplane to the measured cg, the comparison improved, as seen in figures 20, 21, and 22. The comparison of  $\alpha$  also improved for the comparison points near the Mach numbers of 0.93 and 1.18; however, the difference between predicted and measured values increased from a  $\Delta\alpha$  of  $-0.5^\circ$  to  $1.3^\circ$  for the comparison point at the Mach number of 1.06.

The lack of wind-tunnel data and flexibility adjustment probably contributed to the inaccurately predicted pitching moment for this Mach number. However, at the Mach numbers of 0.93 and 1.18, both wind-tunnel data and flexibility corrections were used and significant differences were still obtained. This area requires further investigation if penalties in drag of this magnitude are to be avoided.

Using  $\delta_{e,meas}$  and  $\delta_{c,meas}$  for other Mach numbers did not improve the prediction of drag or angle of attack significantly.

#### SUMMARY OF RESULTS

A program was undertaken by the NASA to evaluate the accuracy of a technique for predicting aerodynamic characteristics of large supersonic cruise airplanes by using small-scale model wind-tunnel data. The method was to compare the flight-measured aerodynamic characteristics of the XB-70-1 airplane for 14 flight conditions with predicted characteristics. Mach numbers ranged from 0.76 to 2.56, with 8 of the 14 conditions concentrated at the transonic Mach numbers and near a Mach number of 2.5.

The predictions were derived from wind-tunnel tests of a 0.03-scale model of the XB-70-1 airplane fabricated to represent the aeroelastically deformed shape at the 2.5 Mach number cruise condition. Corrections for shape differences at the other Mach numbers were included in the prediction.

Although in many of the comparisons the differences between predicted and flight-measured drag were within the combined accuracy of the wind-tunnel tests, the flight test, and the prediction, in some cases large differences were observed. The largest, 27 percent, was at a Mach number of 1.06. Large differences were also observed at a Mach number of 1.18. Some differences in drag appeared to be a function of the lift coefficient since the differences tended to increase with increasing  $C_L$  near Mach numbers of 1.18, 2.1, and 2.5.

There were significant differences in predicted and measured angle of attack for a given  $C_L$  and  $C_M$  at Mach numbers of 0.93, 1.06, and 2.50. The largest differences, from  $0.4^\circ$  to  $0.8^\circ$ , occurred at a Mach number of 2.50, where the most concentrated effort was made to make the best prediction possible.

The differences between predicted and measured elevator deflections were greater than  $2^\circ$  for all the comparison points, except near Mach numbers of 0.76, 1.6, and 2.5. The maximum difference,  $12^\circ$ , occurred at a Mach number of 1.06.

A significant part of the differences in the drag coefficients at the transonic Mach numbers (0.93 to 1.2) was due to the incorrect prediction of the longitudinal control surface deflections required for trim. When  $C_D$  was predicted using measured longitudinal control surface deflections, the agreement improved considerably.

Dryden Flight Research Center  
Edwards, CA 93523  
July 20, 1979

## REFERENCES

1. MacWilkinson, D. G.; Blackerby, W. T.; and Paterson, J. H.: Correlation of Full-Scale Drag Predictions With Flight Measurements on the C-141A Aircraft. Phase 2: Wind Tunnel Test, Analysis, and Prediction Techniques. NASA CR-2333, 1974.
2. Paterson, J. H.; MacWilkinson, D. G.; and Blackerby, W. T.: A Survey of Drag Prediction Techniques Applicable to Subsonic and Transonic Aircraft Design. Aerodynamic Drag, AGARD-CP-124, Oct. 1973, pp. 1-1 - 1-38.
3. Rolls, L. Stewart; and Wingrove, Rodney C.: An Investigation of the Drag Characteristics of a Tailless Delta-Wing Airplane in Flight, Including Comparison With Wind-Tunnel Data. NASA MEMO 10-8-58A, Nov. 1958.
4. Hopkins, Edward J.; Fetterman, David E., Jr.; and Saltzman, Edwin J.: Comparison of Full-Scale Lift and Drag Characteristics of the X-15 Airplane With Wind-Tunnel Results and Theory. NASA TM X-713, 1962.
5. Nissen, James M.; Gadeberg, Burnett L.; and Hamilton, William T.: Correlation of the Drag Characteristics of a Typical Pursuit Airplane Obtained From High-Speed Wind-Tunnel and Flight Tests. NACA TR-916, 1948.
6. Bellman, Donald R.: A Summary of Flight-Determined Transonic Lift and Drag Characteristics of Several Research Airplane Configurations. NASA Memo 3-3-59H, 1959.
7. Saltzman, Edwin J.; and Garringer, Darwin J.: Summary of Full-Scale Lift and Drag Characteristics of the X-15 Airplane. NASA TN D-3343, 1966.
8. Saltzman, Edwin J.; Bellman, Donald R.; and Musialowski, Norman T.: Flight-Determined Transonic Lift and Drag Characteristics of the YF-102 Airplane With Two Wing Configurations. NACA RM H56E08, 1956.
9. Pyle, Jon S.; and Swanson, Robert H.: Lift and Drag Characteristics of the M2-F2 Lifting Body During Subsonic Gliding Flight. NASA TM X-1431, 1967.
10. Pyle, Jon S.: Lift and Drag Characteristics of the HL-10 Lifting Body During Subsonic Gliding Flight. NASA TN D-6263, 1971.
11. Pyle, Jon S.: Preliminary Lift and Drag Characteristics of the F-8 Supercritical Wing Airplane. Supercritical Wing Technology - A Progress Report on Flight Evaluations. NASA SP-301, 1972, pp. 59-70.
12. Baldwin, W.; and Burnett, D.: Flight Demonstration of the TACT Supercritical Wing and Correlation With Wind Tunnel Results. Symposium on Transonic Aircraft Technology (TACT), AFFDL-TR-78-100, 1978, pp. 135-184.
13. Arnaiz, Henry H.; and Schweikhard, William G.: Validation of the Gas Generator Method of Calculating Jet-Engine Thrust and Evaluation of XB-70-1 Airplane Engine Performance at Ground Static Conditions. NASA TN D-7028, 1970.

14. Beaulieu, Warren; Campbell, Ralph; and Burcham, William: Measurement of XB-70 Propulsion Performance Incorporating the Gas Generator Method. J. Aircraft, vol. 6, no. 4, July-Aug. 1969, pp. 312-317.
15. Arnaiz, Henry H.: Flight-Measured Lift and Drag Characteristics of a Large, Flexible, High Supersonic Cruise Airplane. NASA TM X-3532, 1977.
16. Wykes, John H.; and Lawrence, Robert E.: Estimated Performance and Stability and Control Data for Correlation With XB-70-1 Flight Test Data. NASA CR-114335, 1971.
17. Daugherty, James C.: Wind-Tunnel/Flight Correlation Study of Aerodynamic Characteristics of a Large Flexible Supersonic Cruise Airplane (XB-70-1). I - Wind-Tunnel Tests of a 0.03-Scale Model at Mach Numbers From 0.6 to 2.53. NASA TP-1514, 1980.
18. Peterson, John B., Jr.; Mann, Michael J.; Sorrells, Russell B., III; Sawyer, Wallace C.; and Fuller, Dennis E.: Wind-Tunnel/Flight Correlation Study of Aerodynamic Characteristics of a Large Flexible Supersonic Cruise Airplane (XB-70-1). II - Extrapolation of Wind-Tunnel Data to Full-Scale Conditions. NASA TP-1515, 1980.
19. Bertram, Mitchel H.: Calculations of Compressible Average Turbulent Skin Friction. NASA TR R-123, 1962.
20. Fisher, David F.; and Saltzman, Edwin J.: Local Skin Friction Coefficients and Boundary-Layer Profiles Obtained in Flight From the XB-70-1 Airplane at Mach Numbers up to 2.5. NASA TN D-7220, 1973.
21. Hoerner, Sighard F.: Fluid-Dynamic Drag. Publ. by the author (148 Busteed Dr., Midland Park, N.J.), 1958.
22. Conference on Aircraft Operating Problems. NASA SP-83, 1965.
23. Brown, Clinton E.; and Chen, Chuan Fang: An Analysis of Performance Estimation Methods for Aircraft. NASA CR-921, 1967.

TABLE 1.- GEOMETRIC CHARACTERISTICS OF XB-70-1 AIRPLANE

Total wing -		
Total area (includes 230.62 m <sup>2</sup> (2482.34 ft <sup>2</sup> ) covered by fuselage but not 3.12 m <sup>2</sup> (33.53 ft <sup>2</sup> ) of the wing ramp area), m <sup>2</sup> (ft <sup>2</sup> ) . . . . .	585.07	(6297.8)
Span, m (ft) . . . . .	32	(105)
Aspect ratio . . . . .	1.751	
Taper ratio . . . . .	0.019	
Dihedral angle, deg . . . . .	0	
Root chord (wing station 0), m (ft) . . . . .	35.89	(117.76)
Tip chord (wing station 16 m (630 in.)), m (ft) . . . . .	0.67	(2.19)
Mean aerodynamic chord (wing station 5.43 m (17.82 ft)), m (ft) . . . . .	23.94	(78.532)
Fuselage station of 25-percent wing mean aerodynamic chord, m (ft) . . . . .	41.18	(135.10)
Sweepback angle, deg:		
Leading edge . . . . .	65.57	
25-percent element . . . . .	58.79	
Trailing edge . . . . .	0	
Incidence angle, deg:		
Root (fuselage juncture) . . . . .	0	
Tip (fold line and outboard) . . . . .	-2.60	
Airfoil section (modified hexagonal):		
Root to wing station 4.72 m (186 in.) (thickness-chord ratio, 2 percent) . . . . .	0.30 to 0.70	
Wing station 11.68 m (460 in.) to 16.00 m (630 in.) (thickness-chord ratio, 2.5 percent) . . . . .	0.30 to 0.70	
Inboard wing -		
Area (includes 230.62 m <sup>2</sup> (2482.34 ft <sup>2</sup> ) covered by fuselage but not 3.12 m <sup>2</sup> (33.53 ft <sup>2</sup> ) wing ramp area), m <sup>2</sup> (ft <sup>2</sup> ) . . . . .	488.28	(5256.0)
Span, m (ft) . . . . .	19.34	(63.44)
Aspect ratio . . . . .	0.766	
Taper ratio . . . . .	0.407	
Dihedral angle, deg . . . . .	0	
Root chord (wing station 0), m (ft) . . . . .	35.89	(117.76)
Tip chord (wing station 9.67 m (380.62 in.)), m (ft) . . . . .	14.61	(47.94)
Mean aerodynamic chord (wing station 4.15 m (163.58 in.)), m (in.) . . . . .	26.75	(1053)
Fuselage station of 25-percent wing mean aerodynamic chord, m (in.) . . . . .	39.07	(1538.29)
Sweepback angle, deg:		
Leading edge . . . . .	65.57	
25-percent element . . . . .	58.79	
Trailing edge . . . . .	0	

TABLE 1.- Continued

Airfoil section (modified hexagonal):		
Root (thickness-chord ratio, 2 percent)	0.30 to 0.70	
Tip (thickness-chord ratio, 2.4 percent)	0.30 to 0.70	
Mean camber (leading edge), deg:		
Butt plane 0	0.45	
Butt plane 2.72 m (107 in.)	4.40	
Butt plane 3.89 m (153 in.)	2.75	
Butt plane 6.53 m (257 in.)	2.60	
Butt plane 9.32 m (367 in.) to tip	0	
Outboard wing -		
Area (one side only), m <sup>2</sup> (ft <sup>2</sup> )	48.39 (520.90)	
Span, m (ft)	6.33 (20.78)	
Aspect ratio	0.829	
Taper ratio	0.046	
Dihedral angle, deg	5	
Root chord (wing station 9.67 m (380.62 in.)), m (ft)	14.61 (47.94)	
Tip chord (wing station 16.00 m (630 in.)), m (ft)	0.67 (2.19)	
Mean aerodynamic chord (wing station 11.87 m (467.37 in.)), m (in.)	9.76 (384.25)	
Sweepback angle, deg:		
Leading edge	65.57	
25-percent element	58.79	
Trailing edge	0	
Airfoil section (modified hexagonal):		
Root (thickness-chord ratio, 2.4 percent)	0.30 to 0.70	
Tip (thickness-chord ratio, 2.5 percent)	0.30 to 0.70	
Down deflection from wing reference plane, deg	0,25,65	
Skewline of tip fold, deg:		
Leading edge in	1.5	
Leading edge down	3	
		<u>Wingtips</u>
	<u>Up</u>	<u>Down</u>
Elevons (data for one side):		
Total area aft of hinge line, m <sup>2</sup> (ft <sup>2</sup> )	18.37 (197.7)	12.57 (135.26)
Span, m (ft)	6.23 (20.44)	4.26 (13.98)
Inboard chord (equivalent), m (in.)	2.95 (116)	2.95 (116)
Outboard chord (equivalent), m (in.)	2.95 (116)	2.95 (116)
Sweepback angle of hinge line, deg	0	0
Deflection, deg:		
As elevator		-25 to 15
As aileron with elevators at ±15° or less		-15 to 15
As aileron with elevators at -25°		-5 to 5
Total		-30 to 30

TABLE 1.- Continued

## Canard -

Area (includes 13.96 m <sup>2</sup> (150.31 ft <sup>2</sup> ) covered by fuselage), m <sup>2</sup> (ft <sup>2</sup> ) . . . . .	38.61 (415.59)
Span, m (ft) . . . . .	8.78 (28.81)
Aspect ratio . . . . .	1.997
Taper ratio . . . . .	0.388
Dihedral angle, deg . . . . .	0
Root chord (canard station 0), m (ft) . . . . .	6.34 (20.79)
Tip chord (canard station 4.39 m (172.86 in.)), m (ft) . . . . .	2.46 (8.06)
Mean aerodynamic chord (canard station 1.87 m (73.71 in.)), m (in.) . . . . .	4.68 (184.3)
Fuselage station of 25-percent canard mean aerodynamic chord, m (in.) . . . . .	14.06 (553.73)
Sweepback angle, deg:	
Leading edge . . . . .	31.70
25-percent element . . . . .	21.64
Trailing edge . . . . .	-14.91
Incidence angle (nose up), deg . . . . .	0 to 6
Airfoil section (modified hexagonal):	
Root (thickness-chord ratio 2.5 percent) . . . . .	0.34 to 0.66
Tip (thickness-chord ratio 2.52 percent) . . . . .	0.34 to 0.66
Ratio of canard area to wing area . . . . .	0.066
Canard flap (one of two):	
Area (aft of hinge line), m <sup>2</sup> (ft <sup>2</sup> ) . . . . .	5.08 (54.69)
Ratio of flap area to canard semiarea . . . . .	0.263

## Vertical tail (one of two) -

Area (includes 0.83 m <sup>2</sup> (8.96 ft <sup>2</sup> ) blanketed area), m <sup>2</sup> (ft <sup>2</sup> ) . . . . .	21.74 (233.96)
Span, m (ft) . . . . .	4.57 (15)
Aspect ratio . . . . .	1
Taper ratio . . . . .	0.30
Root chord (vertical-tail station 0), m (ft) . . . . .	7.03 (23.08)
Tip chord (vertical-tail station 4.57 m (180 in.)), m (ft) . . . . .	2.11 (6.92)
Mean aerodynamic chord (vertical-tail station 1.88 m (73.85 in.)), m (in.) . . . . .	5.01 (197.40)
Fuselage station of 25-percent vertical-tail mean aerodynamic chord, m (in.) . . . . .	55.59 (2188.50)
Sweepback angle, deg:	
Leading edge . . . . .	51.77
25-percent element . . . . .	45
Trailing edge . . . . .	10.89
Airfoil section (modified hexagonal):	
Root (thickness-chord ratio 3.75 percent) . . . . .	0.30 to 0.70
Tip (thickness-chord ratio 2.5 percent) . . . . .	0.30 to 0.70
Cant angle, deg . . . . .	0
Ratio of vertical tail to wing area . . . . .	0.037

TABLE 1.- Continued

Rudder travel, deg:		
With gear extended . . . . .		±12
With gear retracted . . . . .		±3
Fuselage (includes canopy) -		
Length, m (ft) . . . . .	56.62 (185.75)	
Maximum depth (fuselage station 22.30 m (878 in.)), m (in.) . . . . .	2.72 (106.92)	
Maximum breadth (fuselage station 21.72 m (855 in.)), m (in.) . . . . .	2.54 (100)	
Side area, m <sup>2</sup> (ft <sup>2</sup> ) . . . . .	87.30 (939.72)	
Planform area, m <sup>2</sup> (ft <sup>2</sup> ) . . . . .	110.07 (1184.78)	
Center of gravity:		
Forward limit, percent mean aerodynamic chord . . . . .		19.0
Aft limit, percent mean aerodynamic chord . . . . .		25.0
Duct -		
Length, m (ft) . . . . .	31.96 (104.84)	
Maximum depth (fuselage station 34.93 m (1375 in.)), m (in.) . . . . .	2.31 (90.75)	
Maximum breadth (fuselage station 53.34 m (2100 in.)), m (in.) . . . . .	9.16 (360.70)	
Side area, m <sup>2</sup> (ft <sup>2</sup> ) . . . . .	66.58 (716.66)	
Planform area, m <sup>2</sup> (ft <sup>2</sup> ) . . . . .	217.61 (2342.33)	
Inlet captive area (each), m <sup>2</sup> (in <sup>2</sup> ) . . . . .	3.61 (5600)	
Surface areas (net wetted), m <sup>2</sup> (ft <sup>2</sup> ) -		
Fuselage, canopy, boundary layer gutter, and tailpipes . . . . .	264.77 (2850.0)	
Duct . . . . .	318.71 (3430.6)	
Wing, wingtips, and wing ramp . . . . .	864.71 (9307.7)	
Vertical tails (two) . . . . .	87.12 (937.7)	
Canard . . . . .	49.47 (532.5)	
Total . . . . .	1584.79 (17,058.5)	
Engines (six) . . . . .		YJ93-GE-3
Boattail angle, deg -		
Upper surface . . . . .		6
Lower surface . . . . .		5
Side . . . . .		6
Base areas, m <sup>2</sup> (ft <sup>2</sup> ) -		
Total . . . . .	12.7 (137)	
Total (all engines on, minimum exit area) . . . . .	10 (107.2)	
Total (all engines on, maximum exit area) . . . . .	4.5 (48.5)	

TABLE 1.- Concluded

Projected thickness (height) of base, m (in.) . . . . .	1.47 (58)
Width of propulsion package, cm (in.) . . . . .	914 (360)
Engine -	
Jet-exit area (minimum), cm <sup>2</sup> (in <sup>2</sup> ) . . . . .	4613 (715)
Jet-exit area (maximum), cm <sup>2</sup> (in <sup>2</sup> ) . . . . .	13,678 (2120)
Jet-exit diameter (minimum), cm (in.) . . . . .	77 (30.2)
Jet-exit diameter (maximum), cm (in.) . . . . .	132 (52)

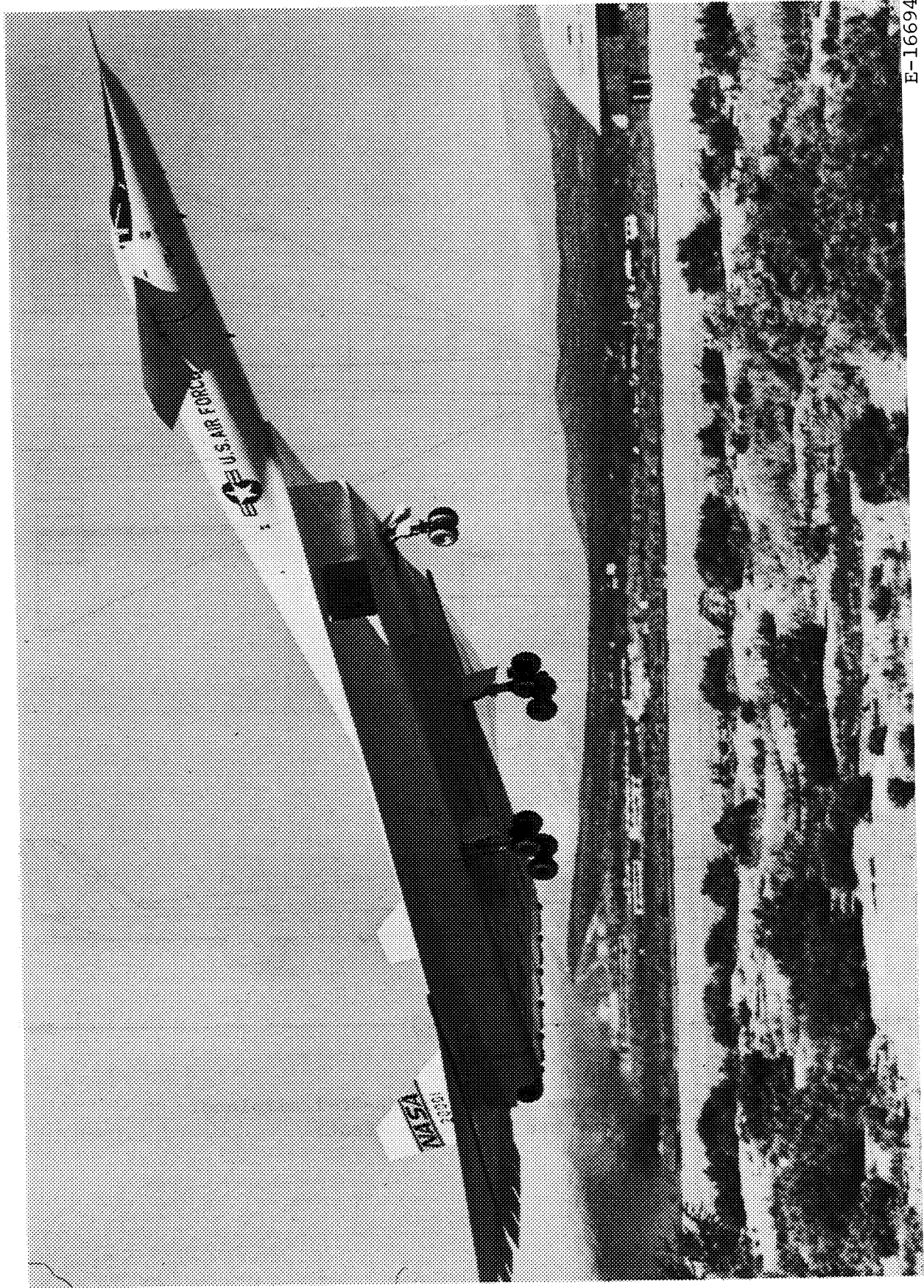
TABLE 2.- SUMMARY OF THE CONFIGURATIONS AND AERODYNAMIC CHARACTERISTICS OF THE  
XB-70-1 AIRPLANE AT THE FLIGHT CONDITIONS OF THE 14 COMPARISON POINTS

Comparison point no.	$M_\infty$	Altitude, m (ft)	$q_\infty'$ , N/m <sup>2</sup> (lb/ft <sup>2</sup> )	$t_\infty'$ , K (°R)	$R_{MAC}$	$\alpha_{meas}'$ , deg	$C_{L,meas}$	$C_{D,meas}$
P1	0.76	7,842 (25,730)	14,684 (306.7)	240.2 (432.3)	$191.3 \times 10^6$	4.4	0.1664	0.01817
P2	0.93	9,988 (32,770)	16,030 (334.8)	235.9 (424.6)	174.3	5.7	0.2299	0.02528
P10	1.06	8,272 (27,140)	26,813 (560.0)	247.4 (445.3)	242.0	3.9	0.1216	0.0272
P3	1.18	10,278 (33,720)	24,478 (511.3)	232.5 (418.5)	216.5	3.2	0.1073	0.02367
P3L	1.15	10,400 (34,121)	23,130 (483.1)	232.2 (417.9)	208.7	2.2	0.0729	0.02256
P3H	1.17	10,046 (32,960)	25,232 (527.0)	234.4 (422.0)	221.3	4.4	0.1528	0.02658
P4	1.61	11,756 (38,570)	36,355 (759.3)	207.7 (373.8)	269.1	3.1	0.0821	0.01746
P5	1.67	12,807 (42,020)	33,260 (694.7)	212.5 (382.5)	231.2	2.9	0.0846	0.01686
P6	2.10	14,813 (48,600)	38,297 (799.8)	210.5 (378.9)	216.5	2.9	0.0765	0.01347
P7	2.15	17,563 (57,620)	26,037 (543.8)	207.9 (374.2)	147.3	4.3	0.1062	0.01752
P8	2.53	19,187 (62,950)	27,801 (580.6)	210.9 (379.6)	133.0	4.7	0.0984	0.01520
P8L	2.51	19,205 (63,010)	27,257 (569.3)	211.1 (380.0)	130.0	3.7	0.0798	0.01261
P8H	2.56	19,224 (63,070)	28,468 (594.6)	208.3 (374.9)	134.5	6.7	0.1405	0.02339
P9	2.50	18,784 (61,630)	28,966 (605.0)	213.8 (384.8)	137.8	4.6	0.0978	0.01523

Comparison point no.	Pitch rate, deg/sec	cg, percent MAC	$\delta_t(\text{left})'$ , deg	$\delta_t(\text{right})'$ , deg	$\delta_c'$ , deg	$\delta_e'$ , deg	$\delta_{byp}'$ , deg	Load factor, g	Shaker vane	Nose ramp
P1	0	24.1	-1.0	-0.5	2.26	2.7	0	1.02	On	Down
P2	0	21.9	23.0	24.7	2.15	2.4	0	1.02	On	Down
P10	0	22.3	24.0	24.0	0.51	12.4	1.5	1.00	Off	Down
P3	0	22.3	23.8	25.3	0.90	10.4	3.2	1.02	On	Down
P3L	-0.55	21.5	23.2	24.7	0.41	12.8	3.4	0.66	On	Down
P3H	0.83	21.0	23.2	24.8	1.61	6.8	3.2	1.51	On	Down
P4	0	21.7	60.0	63.7	1.14	9.7	3.3	1.00	On	Down
P5	0	22.0	64.9	67.2	1.38	9.3	2.8	1.00	On	Down
P6	0	21.1	60.8	63.8	1.98	6.2	7.4	1.00	On	Down
P7	0	21.1	63.4	61.7	2.59	3.7	6.8	1.05	Off	Down
P8	0	21.8	63.9	62.9	2.82	3.2	1.8	0.98	On	Up
P8L	-0.18	20.5	64.2	62.5	2.70	4.6	2.1	0.81	On	Up
P8H	0.57	20.5	64.0	62.2	4.07	-5.2	2.1	1.50	On	Up
P9	0	21.6	61.1	63.2	2.76	3.0	3.8	1.00	On	Down

TABLE 3.- PREDICTED VALUES FOR THE AERODYNAMIC CHARACTERISTICS FOR THE 14 COMPARISON POINTS

	Comparison point number													
	P1	P2	P10	P3	P3L	P3H	P4	P5	P6	P7	P8	P8L	P8H	P9
Mach number	0.76	0.93	1.06	1.18	1.15	1.17	1.61	1.67	2.10	2.15	2.53	2.51	2.56	2.50
$C_{L,meas}$ or $C_{L,pred}$	0.1664	0.2299	0.1216	0.1073	0.0729	0.1528	0.0821	0.0846	0.0765	0.1062	0.0984	0.0798	0.1405	0.0978
$C_{M,meas}$ or $C_{M,pred}$	0.00150	0.00713	0.00328	0.00290	0.00255	0.00611	0.00271	0.00254	0.00298	0.00414	0.00315	0.00359	0.00632	0.00333
$C_{D,pred}$	0.01770	0.02780	0.01964	0.02095	0.02117	0.02400	0.01727	0.01720	0.01410	0.01650	0.01480	0.01282	0.02110	0.01473
$\alpha_{pred}$	4.7	6.3	3.4	3.3	2.5	4.5	3.0	3.1	3.0	4.4	4.1	3.3	5.9	4.0
$\delta_{e,pred}$	1.5	-1.2	0.7	6.7	9.7	1.5	7.7	7.9	1.9	-0.6	1.9	2.9	-5.5	0.9
$\delta_{c,pred}$	2.44	2.68	2.27	1.54	0.88	2.41	1.44	1.59	2.63	3.24	3.01	2.96	4.12	3.08



E-16694

Figure 1.- XB-70-1 airplane.

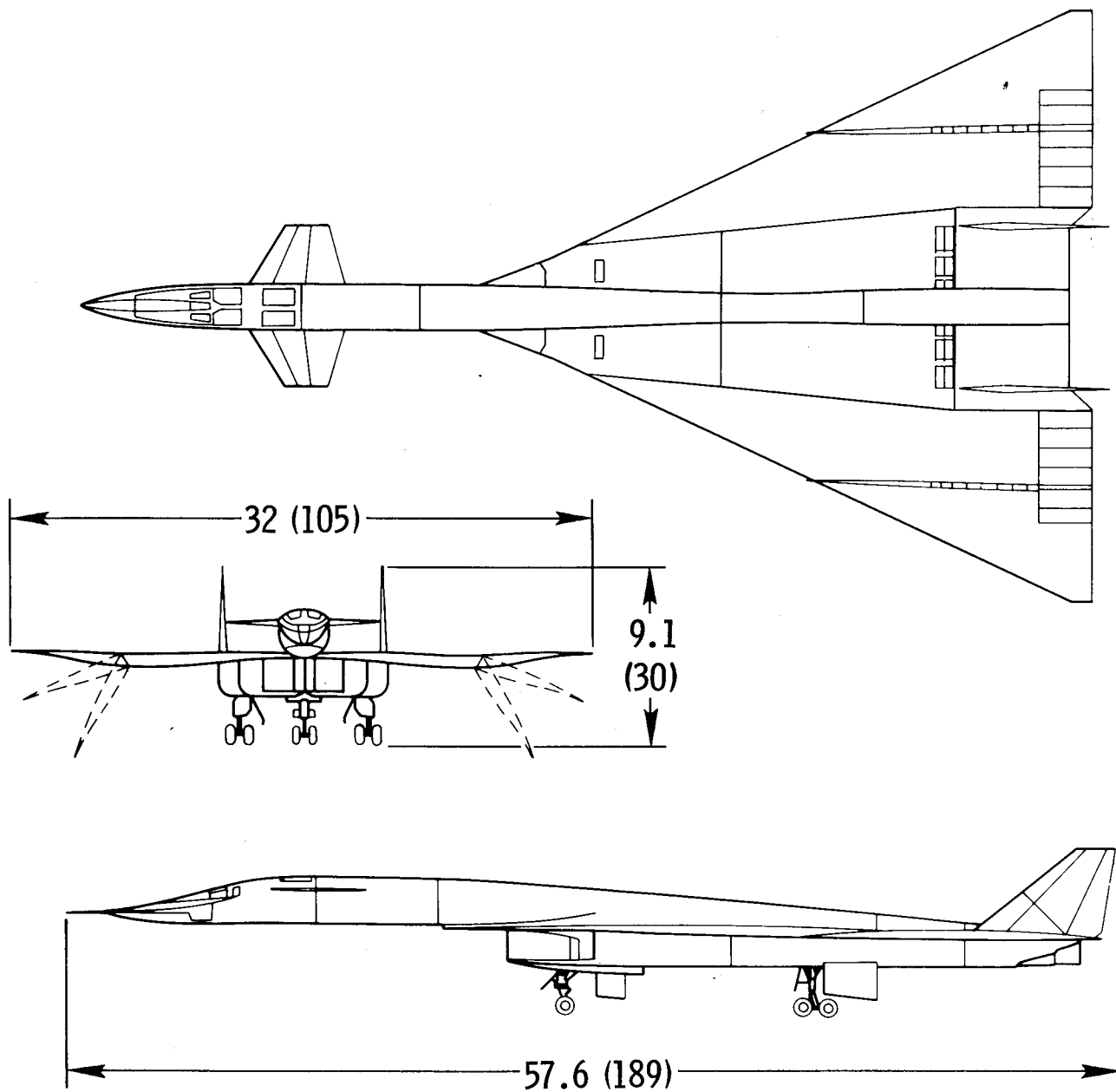


Figure 2.- Three-view drawing of XB-70-1 airplane.  
Dimensions are in meters (feet).

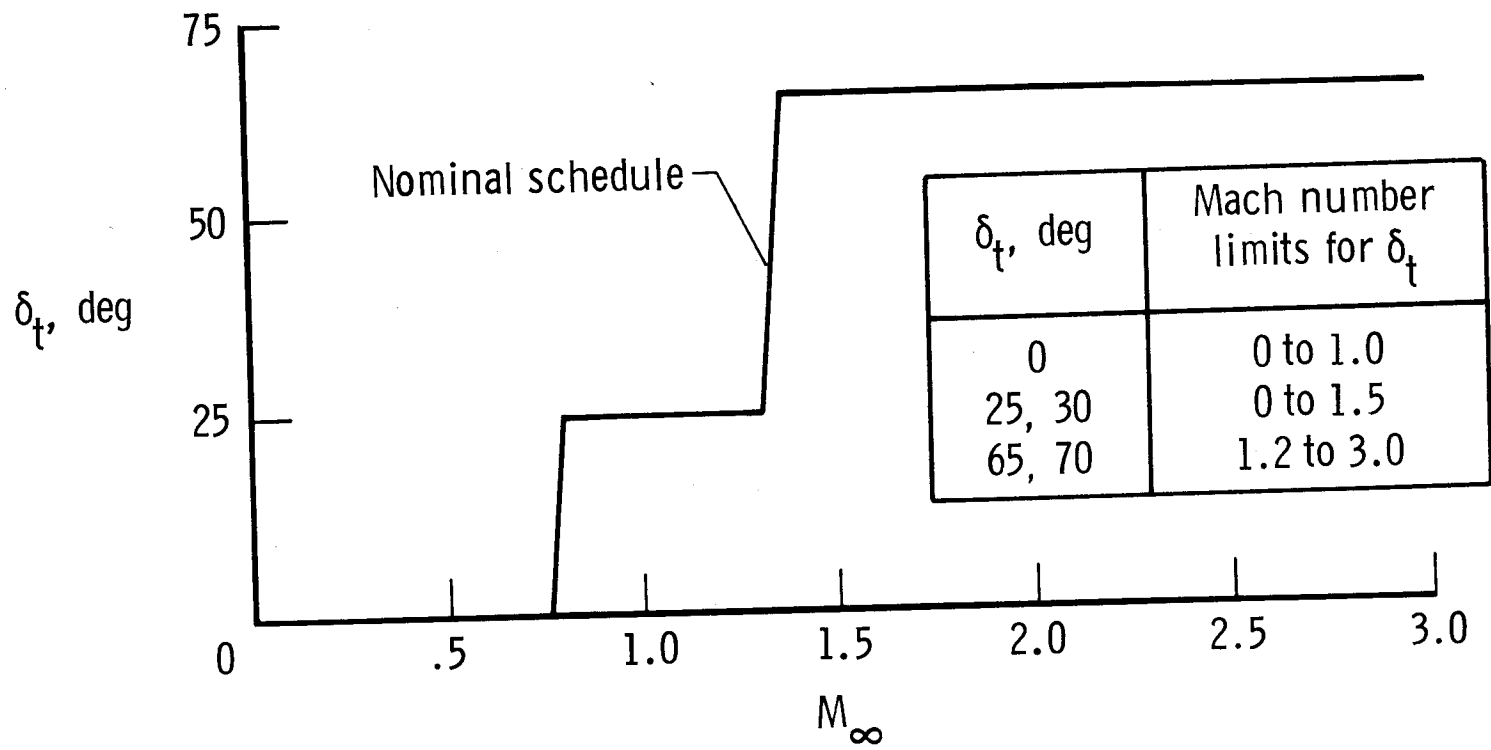


Figure 3.- Nominal folding schedule and operating limits for wingtip positions.

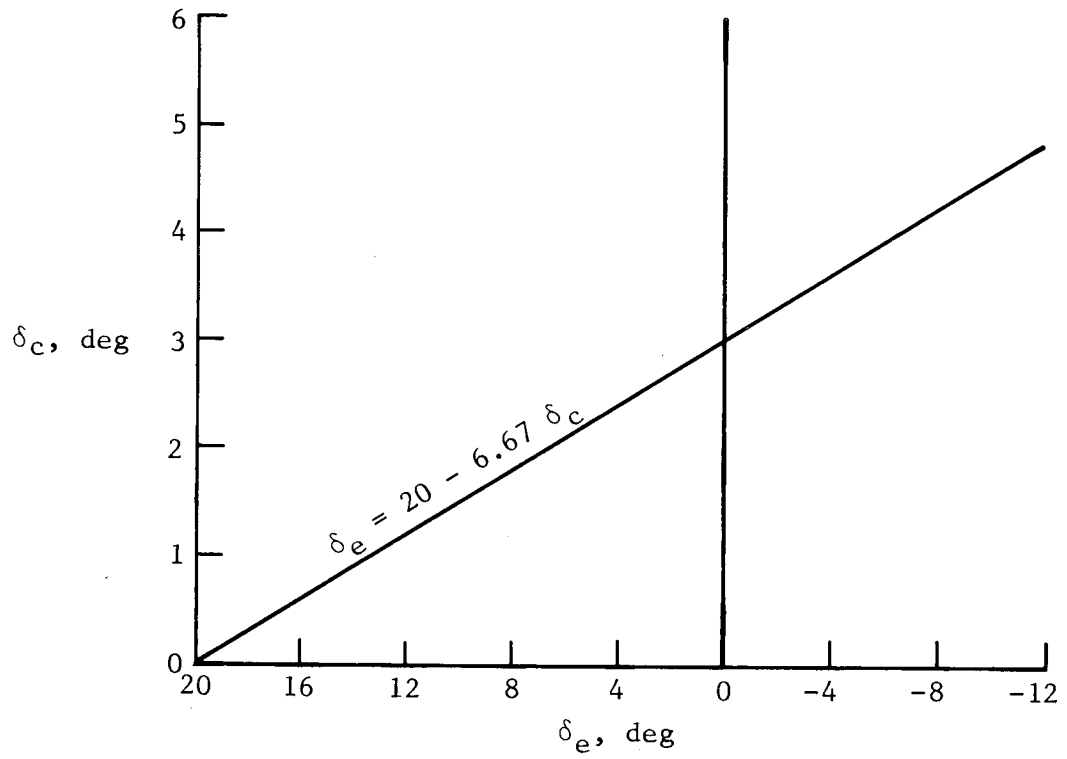


Figure 4.- Elevator-to-canard gearing curve as designed for XB-70-1.

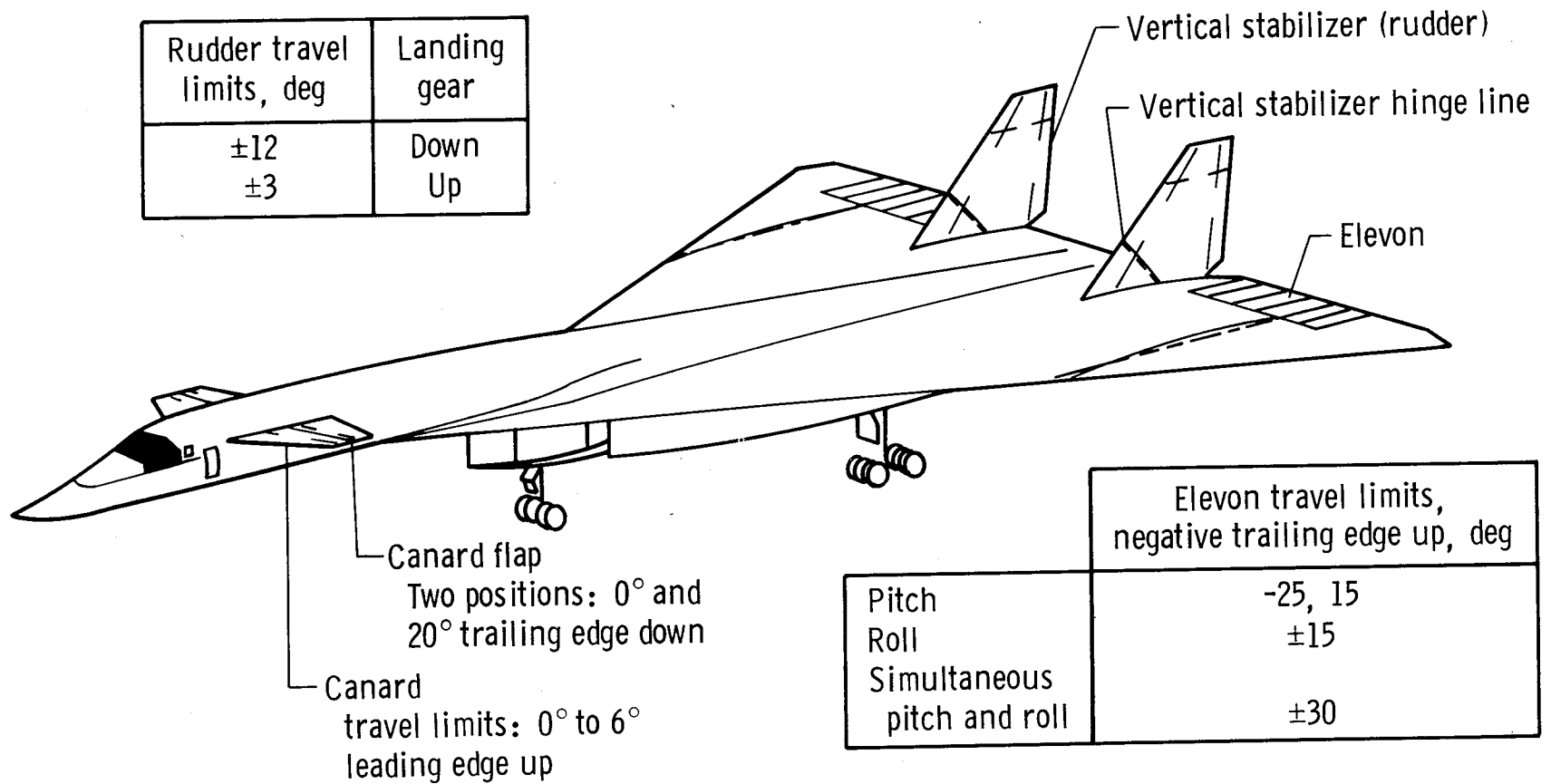


Figure 5.- Control surface locations and deflection limits.

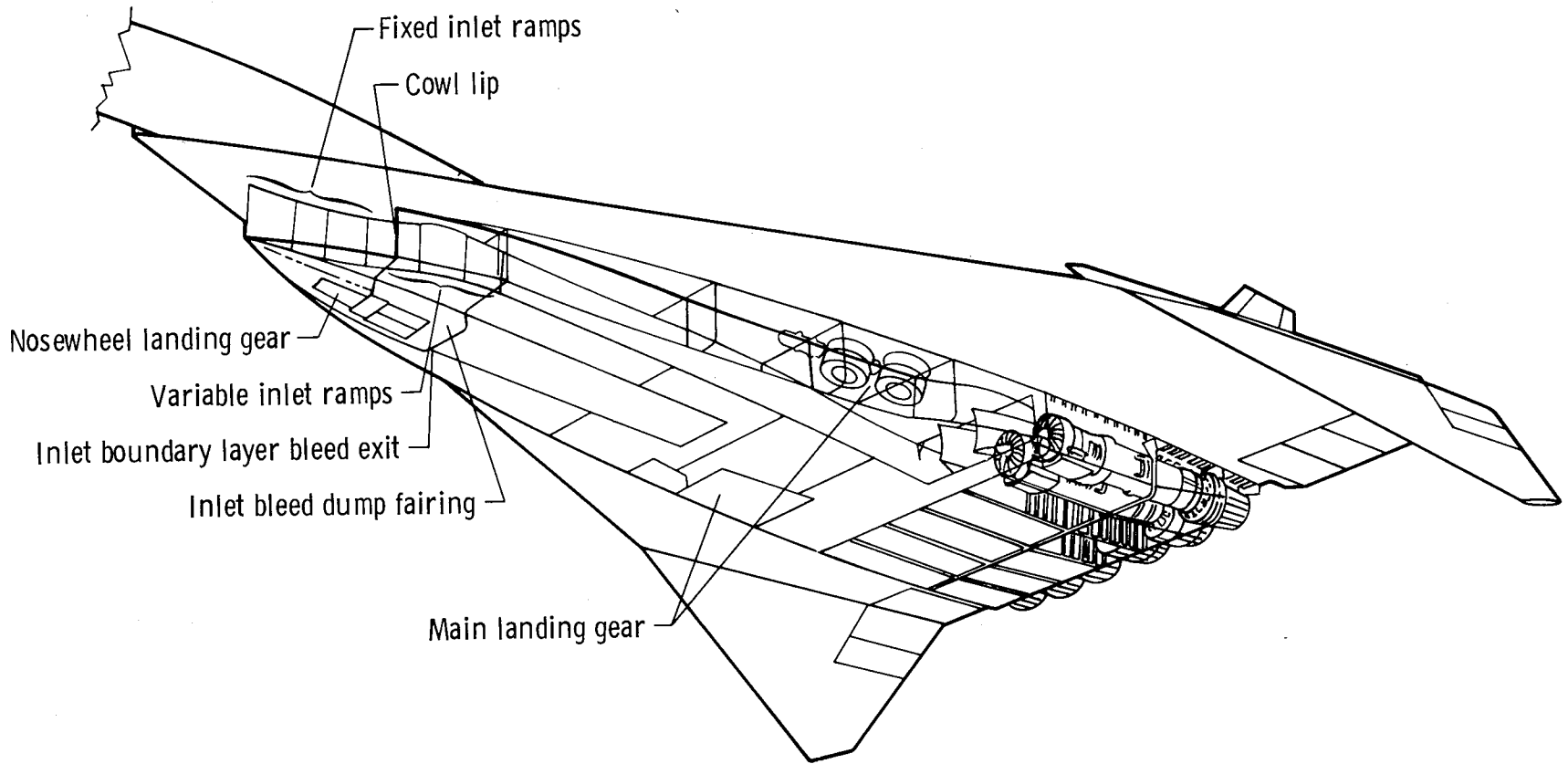


Figure 6.- Propulsion system.

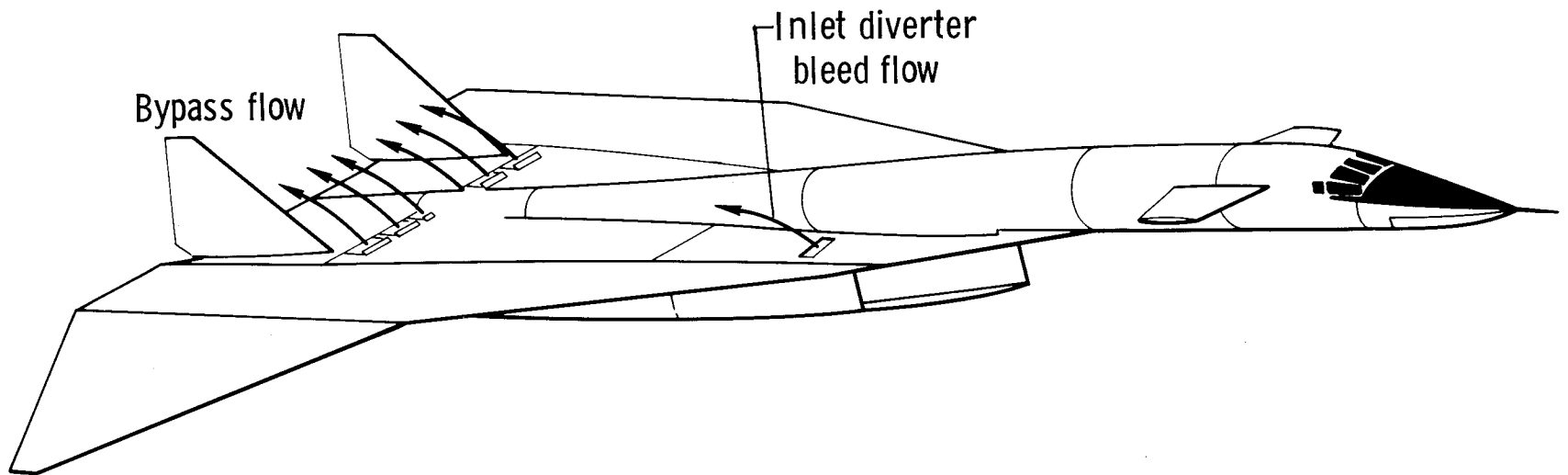
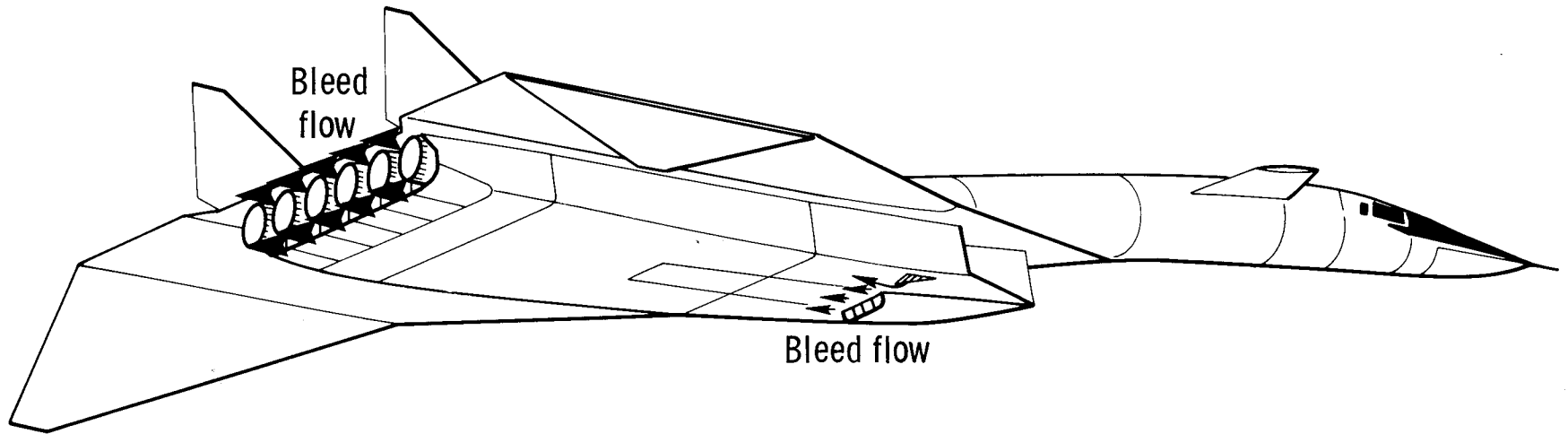
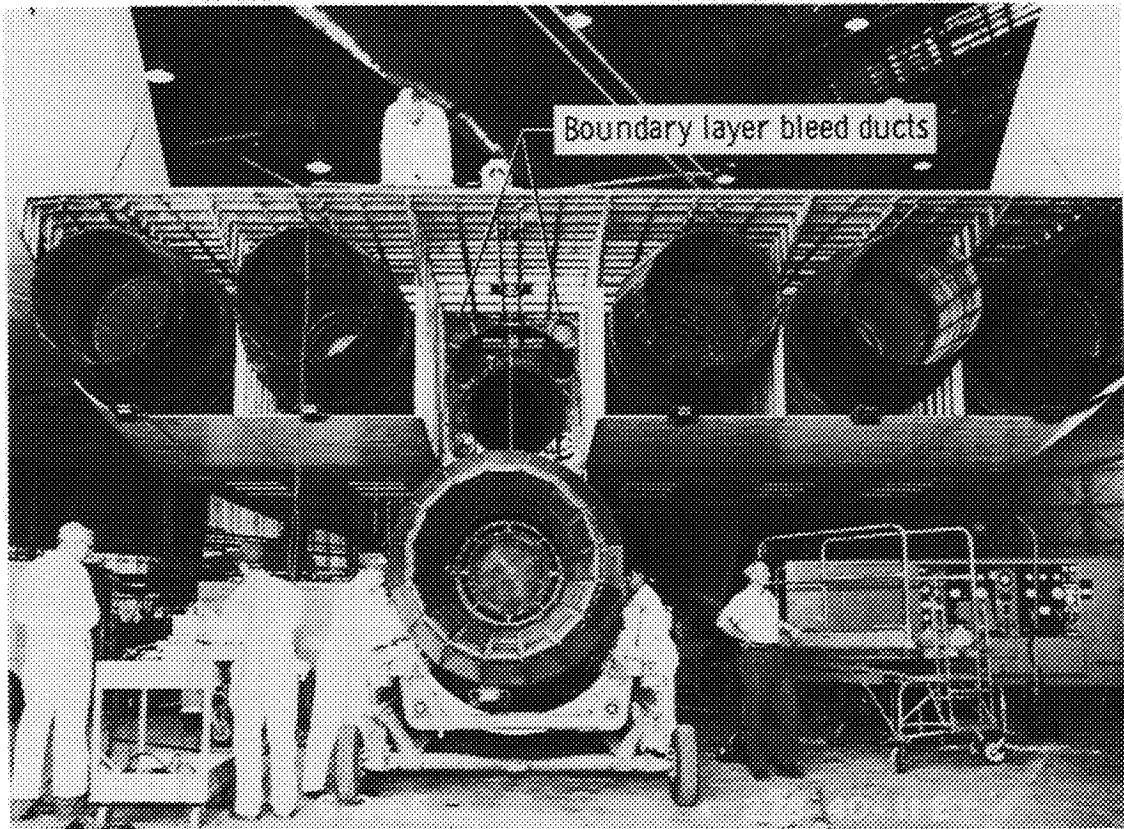
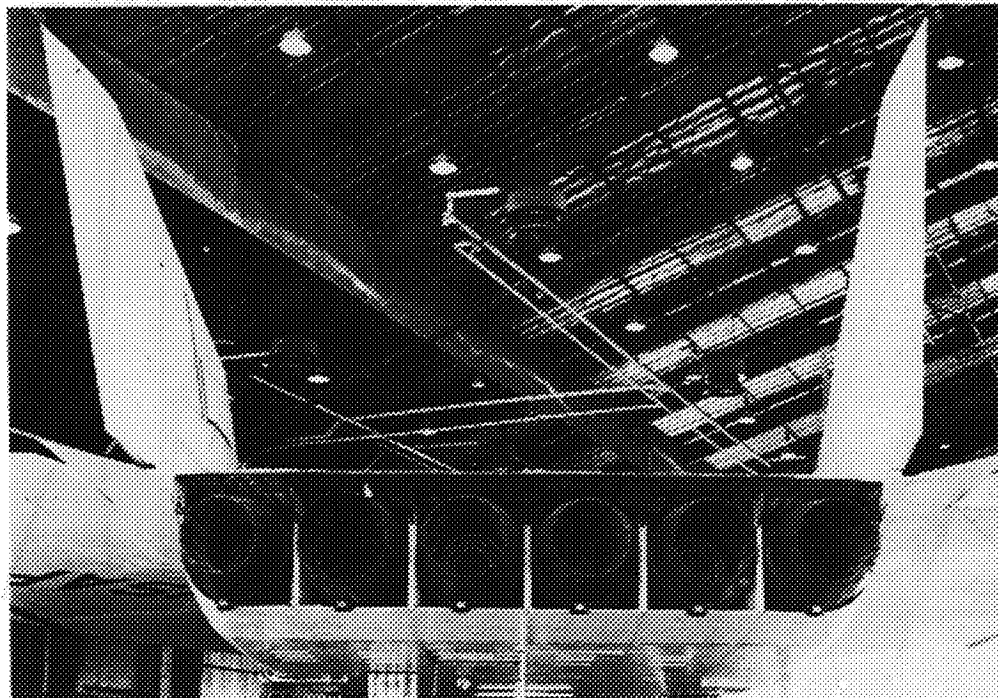


Figure 7.- Exits for inlet bypass and boundary layer bleed flow.



(a) Engine removed showing boundary layer bleed duct exits.



E-17194

(b) Airplane base region.

Figure 8.- Airplane base region and detail.

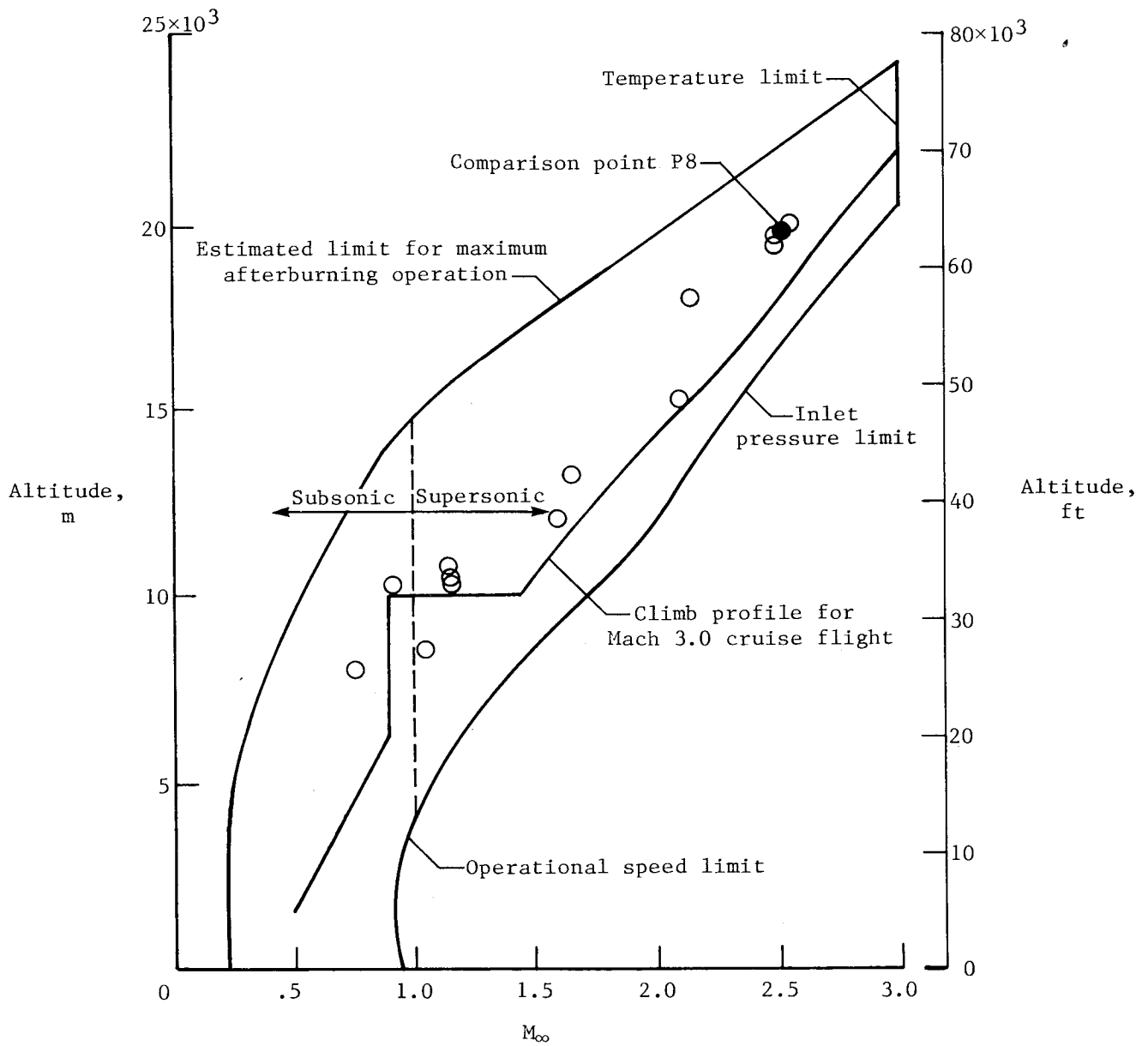


Figure 9.- Operational flight envelope of XB-70-1 airplane showing Mach/altitude of comparison points.

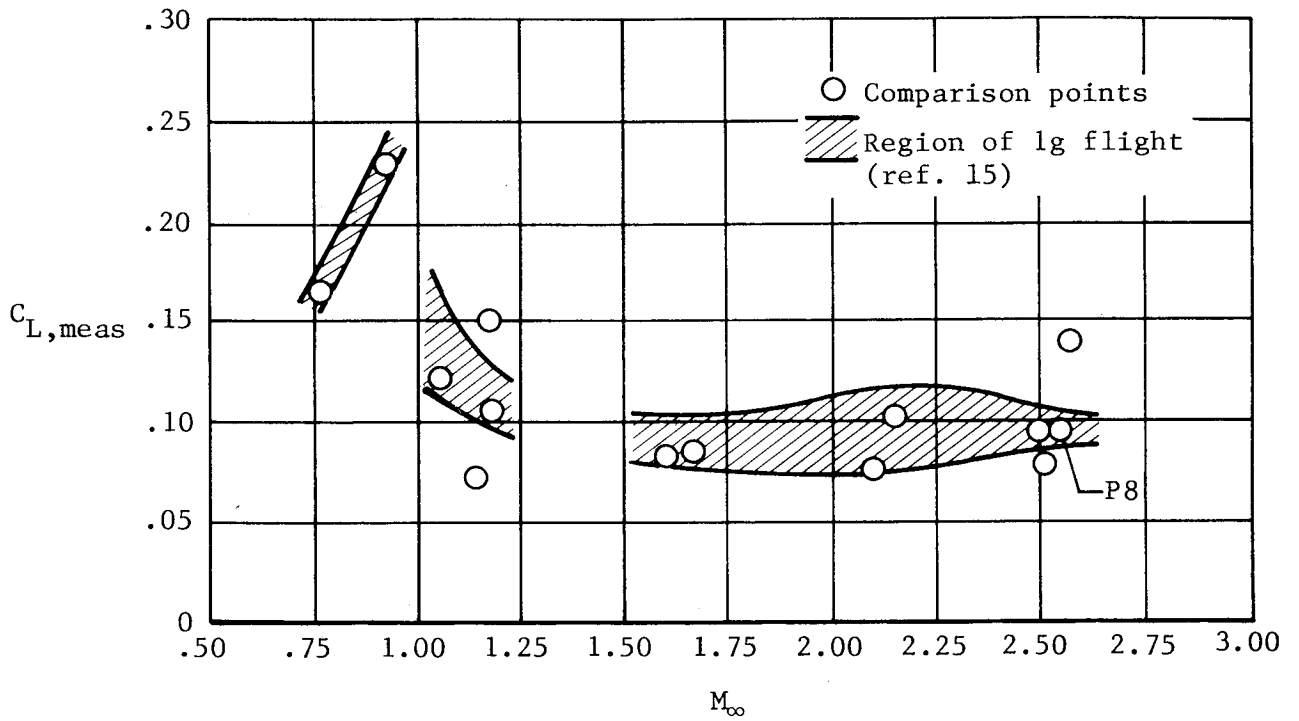
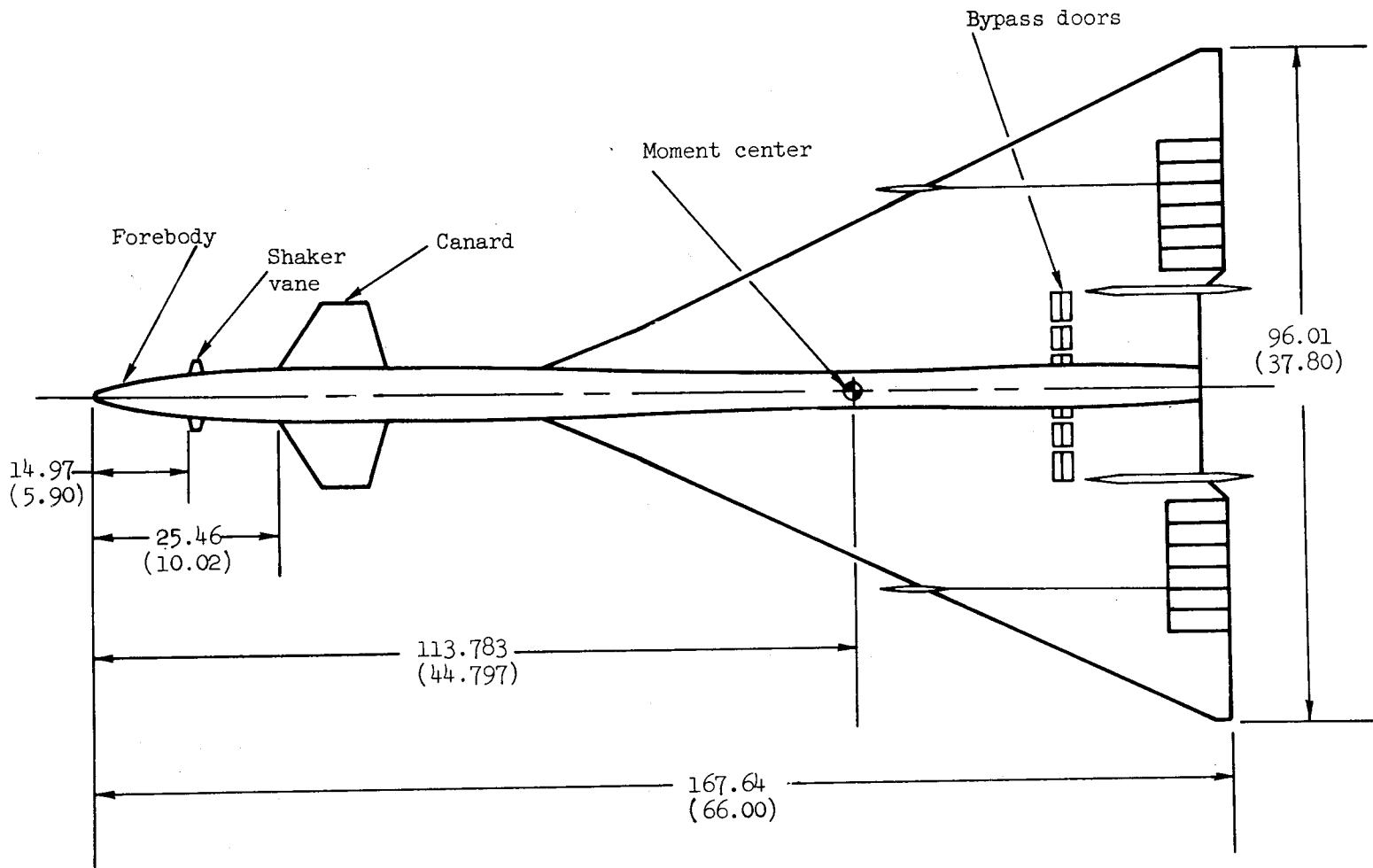
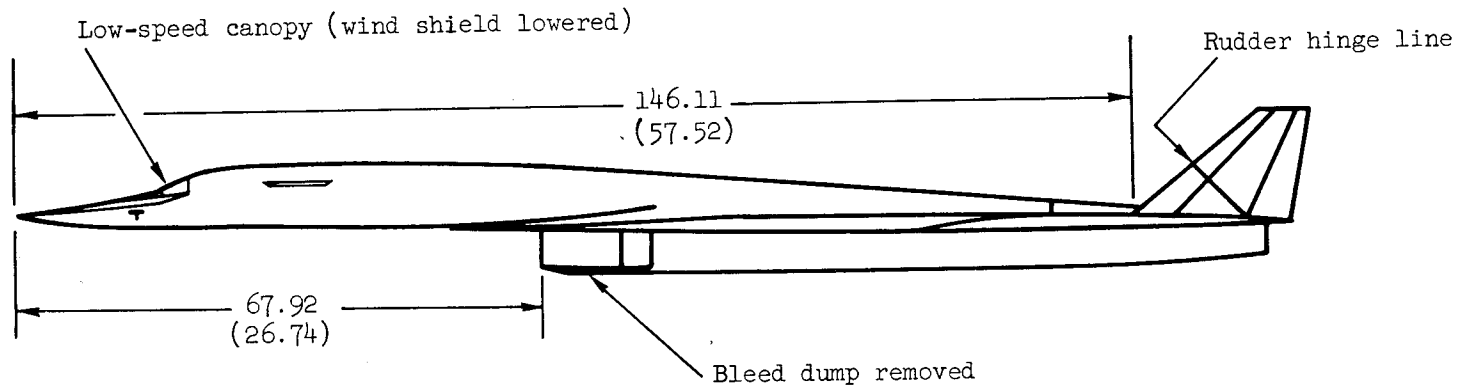


Figure 10.- Variation of  $C_{L,meas}$  with  $M_\infty$  for comparison points with respect to lg flight of XB-70-1 airplane (ref. 15).

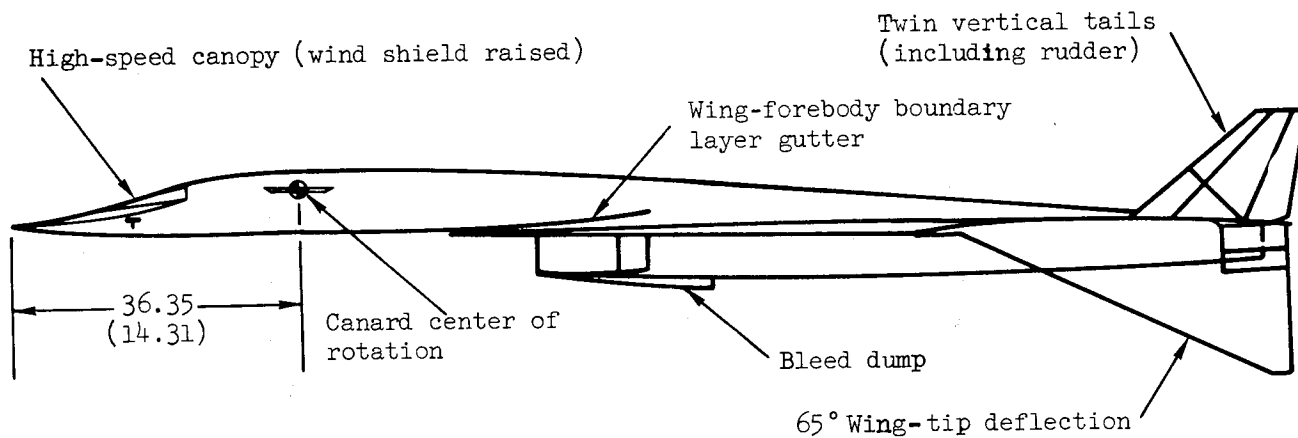


(a) Top view.

Figure 11.- Model drawing.

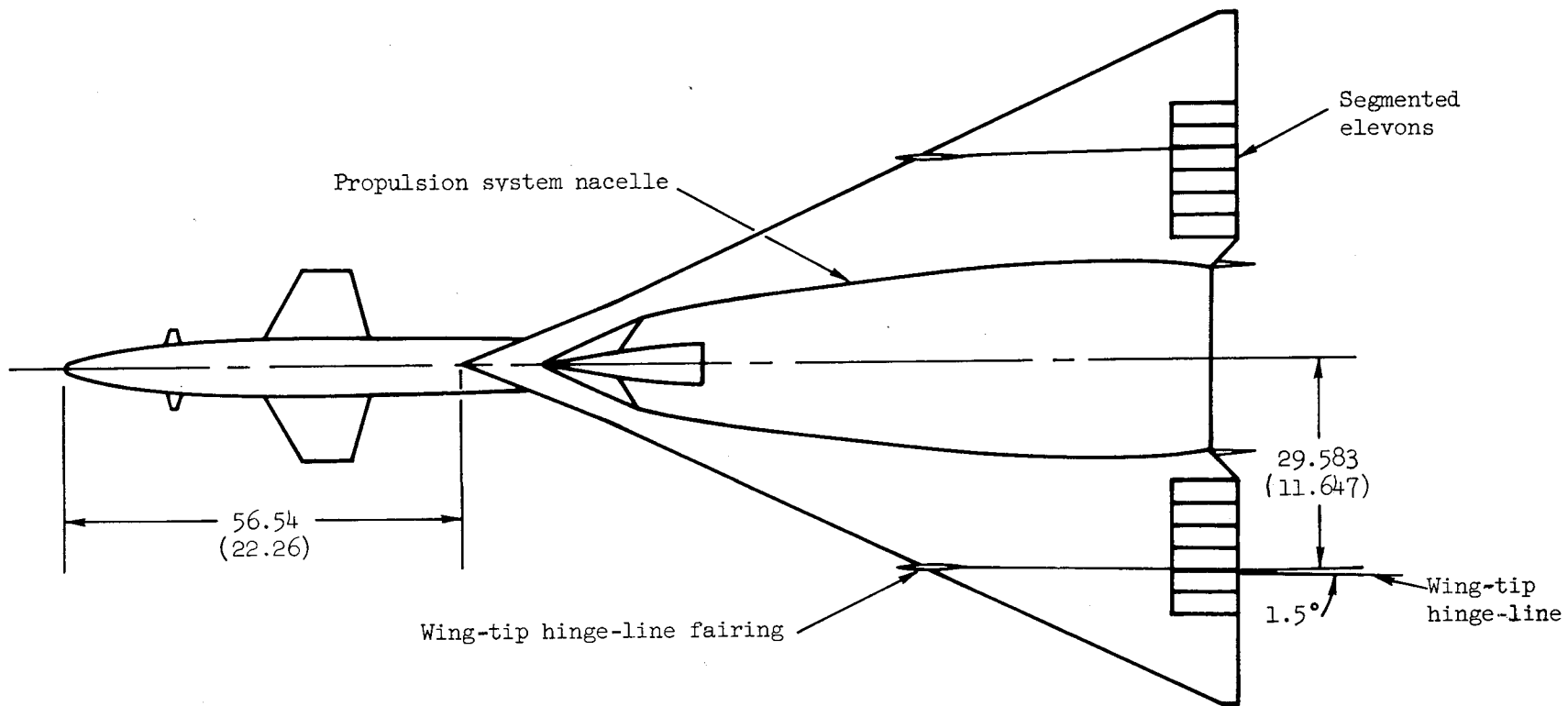


Note: All dimensions are in centimeters (inches)



(b) Side views.

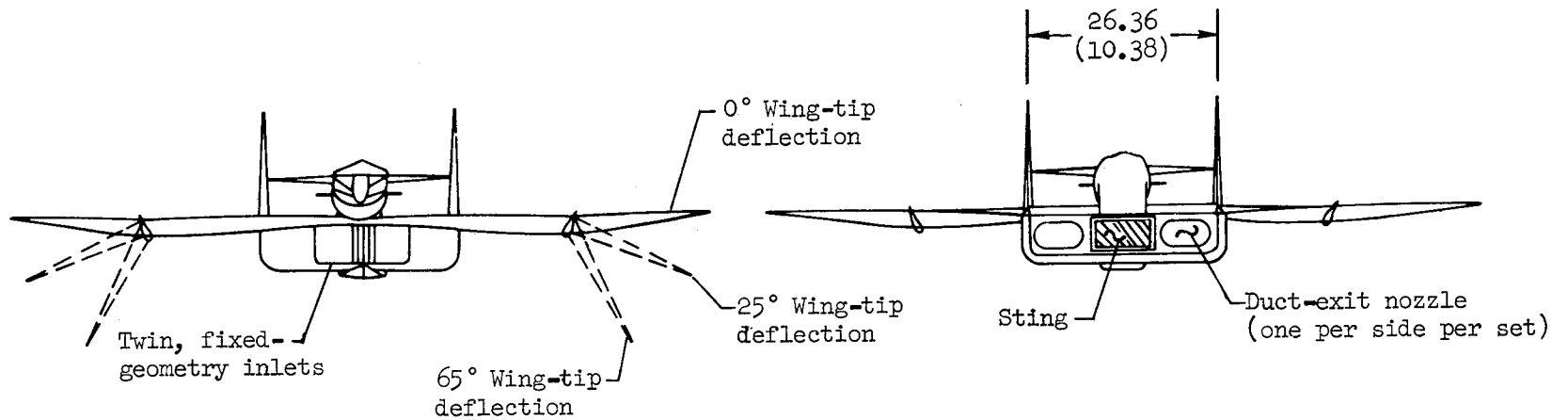
Figure 11.- Continued.



(c) Bottom view.

Figure 11.- Continued.

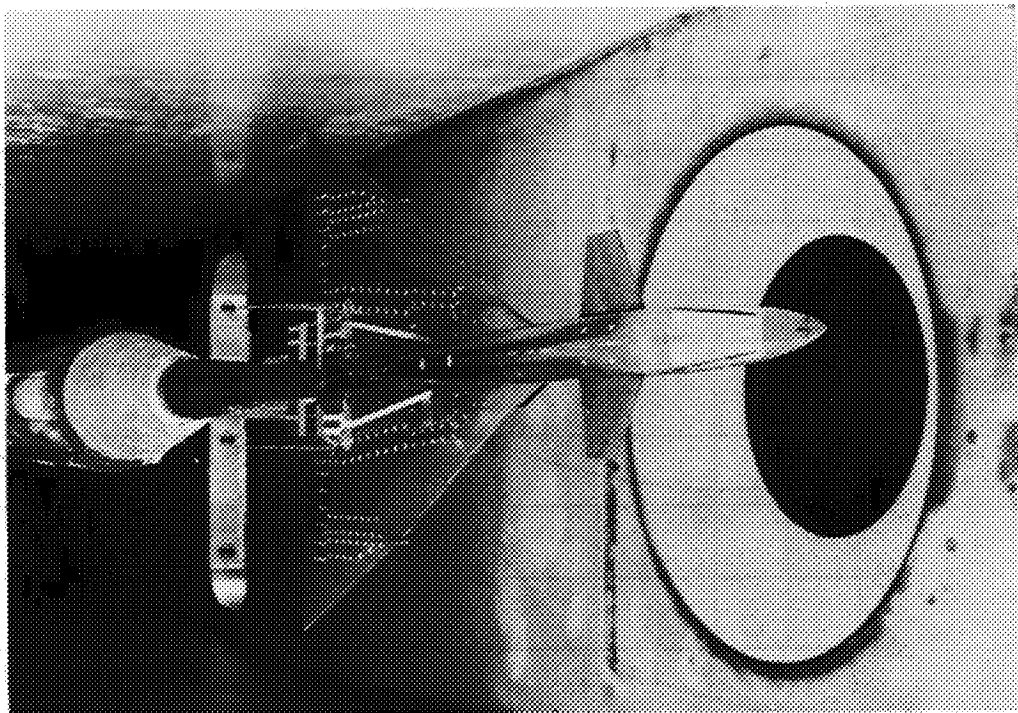
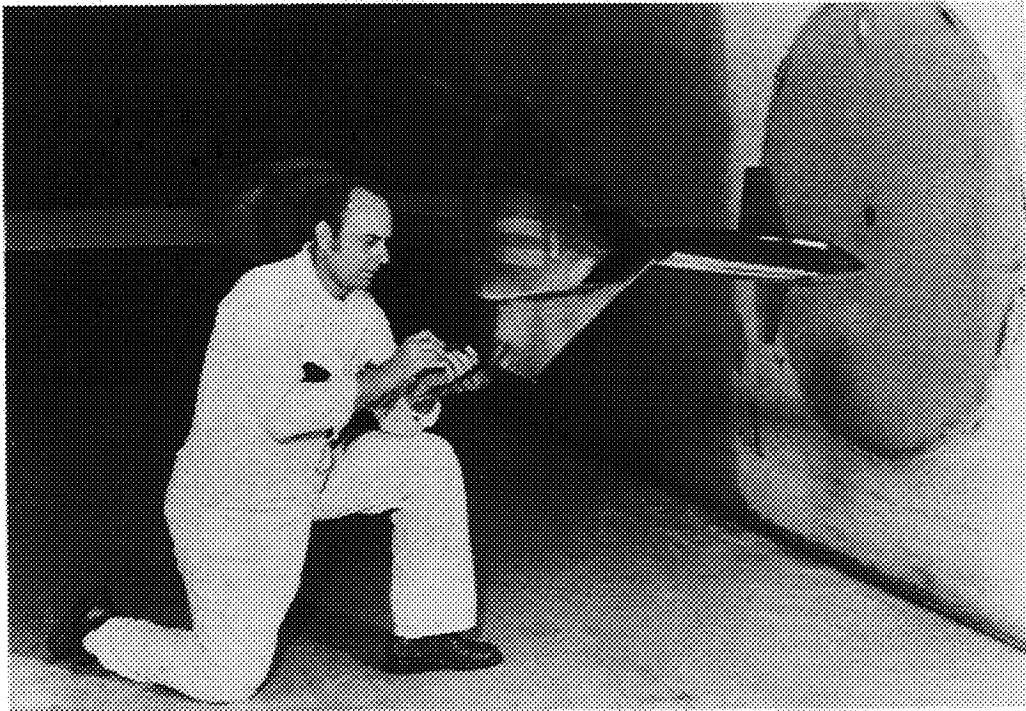
Note: All dimensions are in  
centimeters (inches)



(d) Front view.

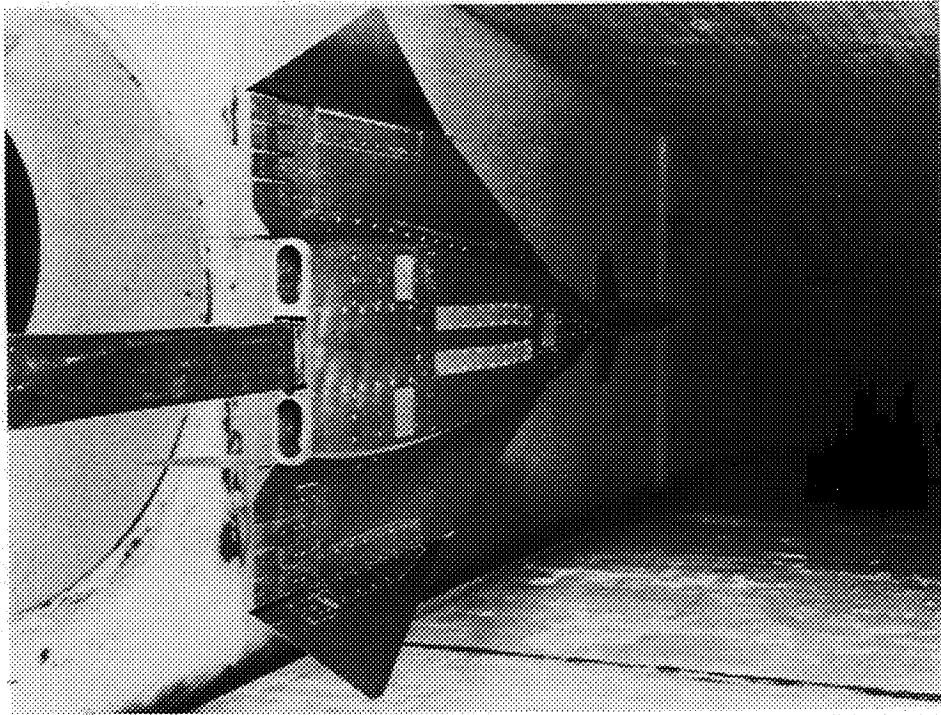
(e) Rear view.

Figure 11.- Concluded.



A70-4983

Figure 12.- Model of XB-70-1 airplane installed in Unitary Plan Wind Tunnel Facility at Ames Research Center.



A71-1925

Figure 12.- Concluded.

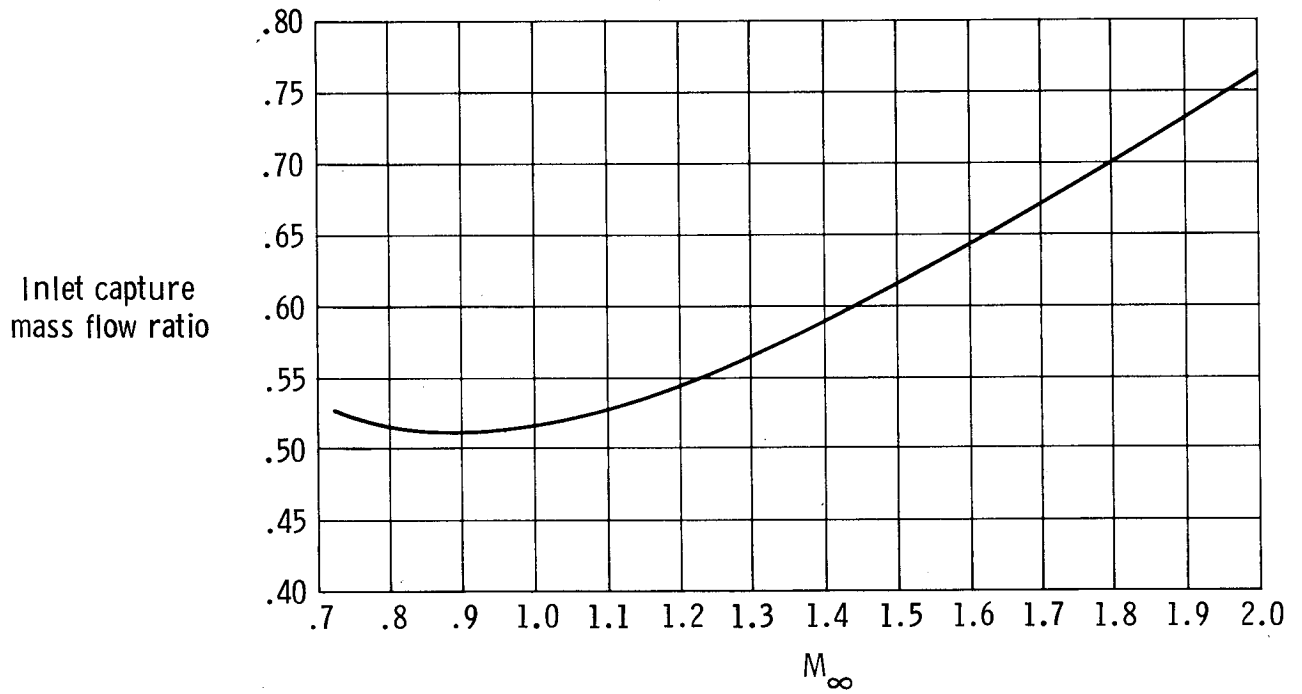
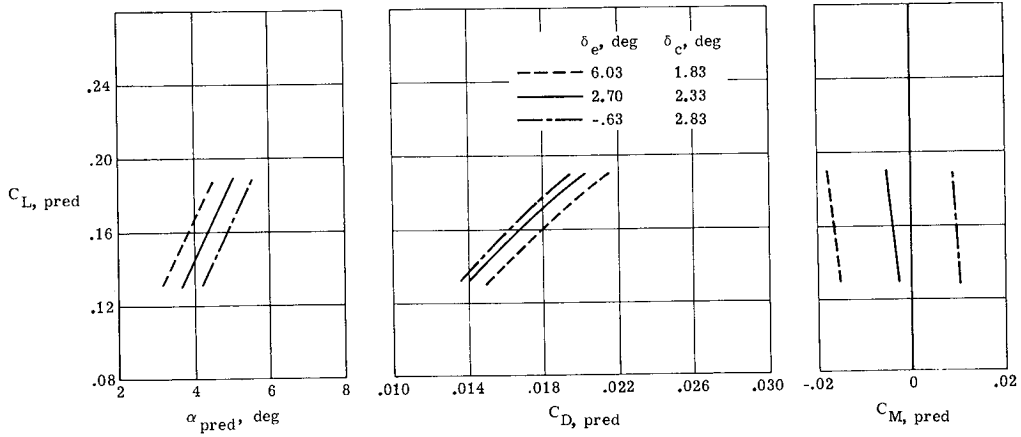
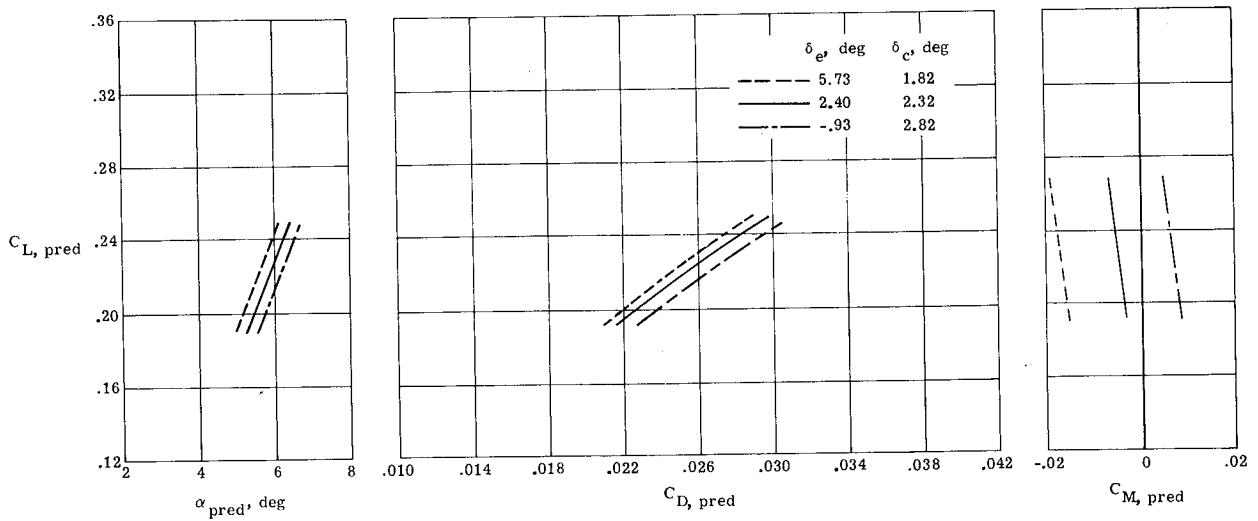


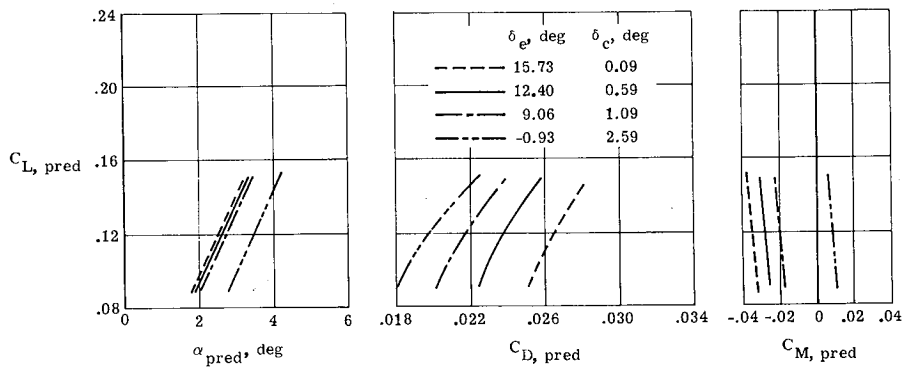
Figure 13.- Reference inlet mass flow ratio for XB-70-1 airplane based on flight-measured values for nominal flight conditions (ref. 15).



(a) Comparison point P1,  $M_\infty = 0.76$ .

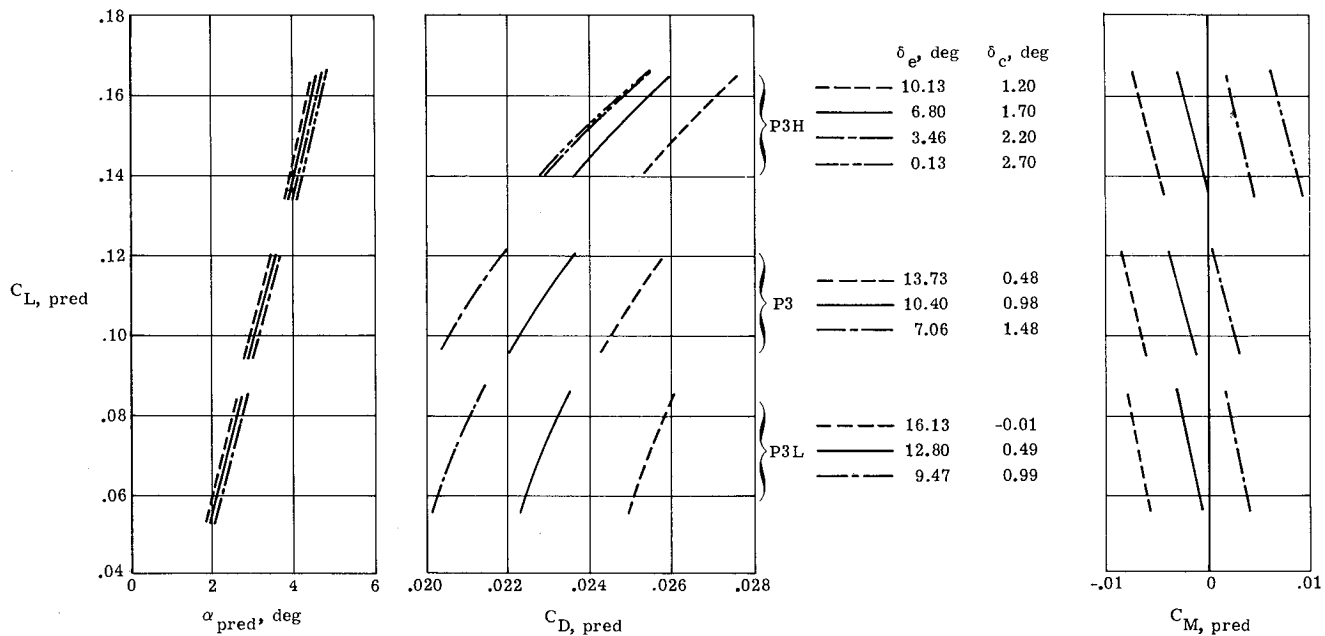


(b) Comparison point P2,  $M_\infty = 0.93$ .

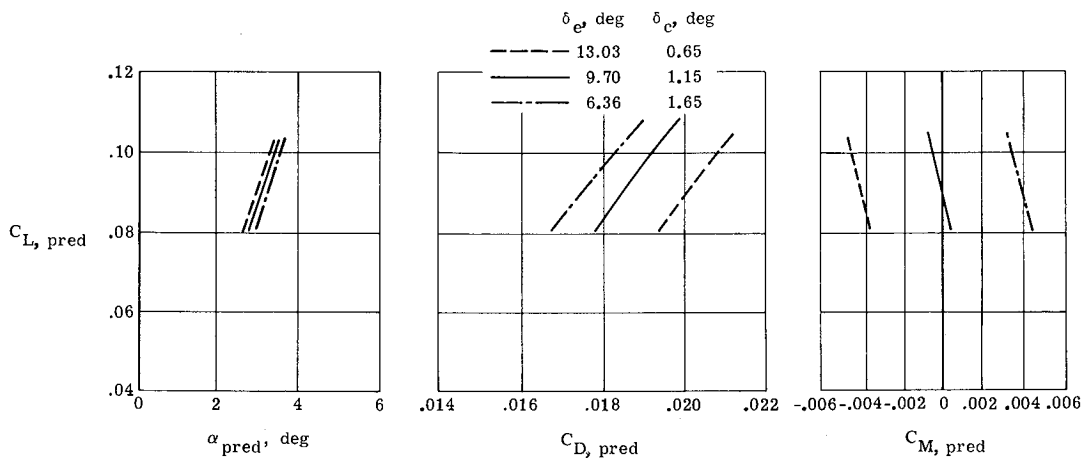


(c) Comparison point P10,  $M_\infty = 1.06$ .

Figure 14.- Predicted aerodynamic characteristics for various elevator/canard deflection combinations for 14 comparison points.

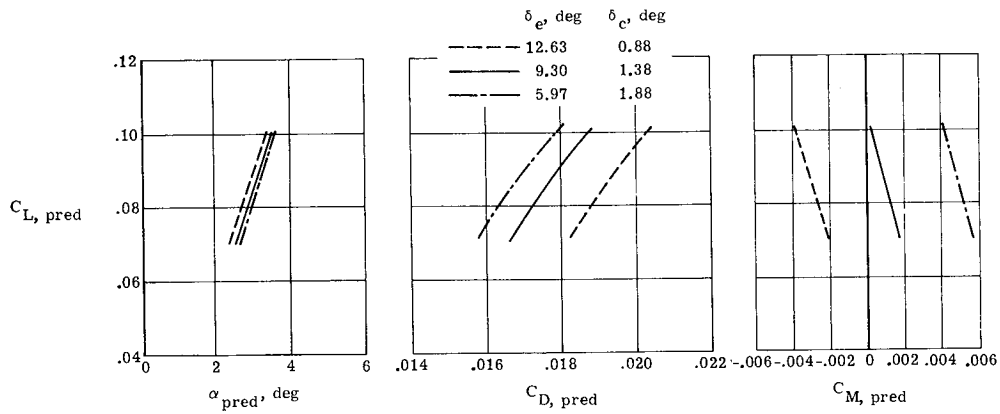


(d) Comparison points P3, P3L, and P3H,  $M_\infty \approx 1.18$ .

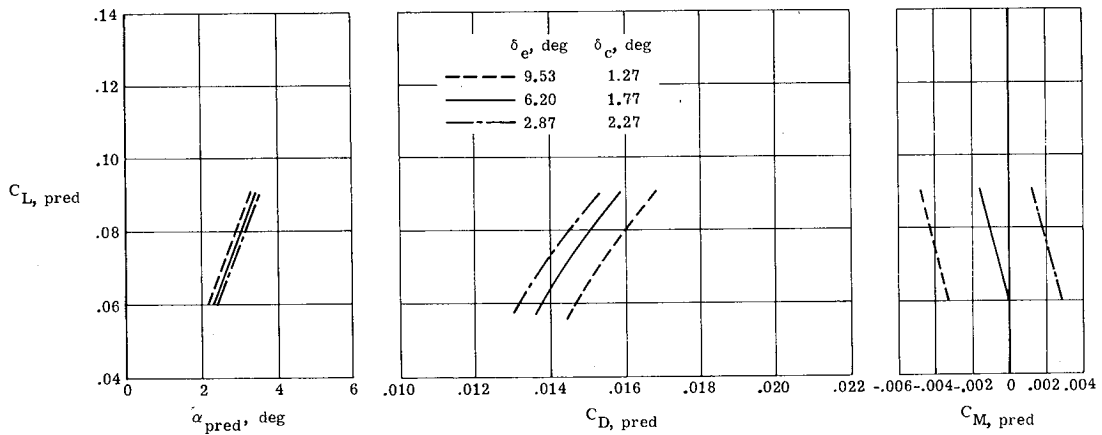


(e) Comparison point P4,  $M_\infty = 1.61$ .

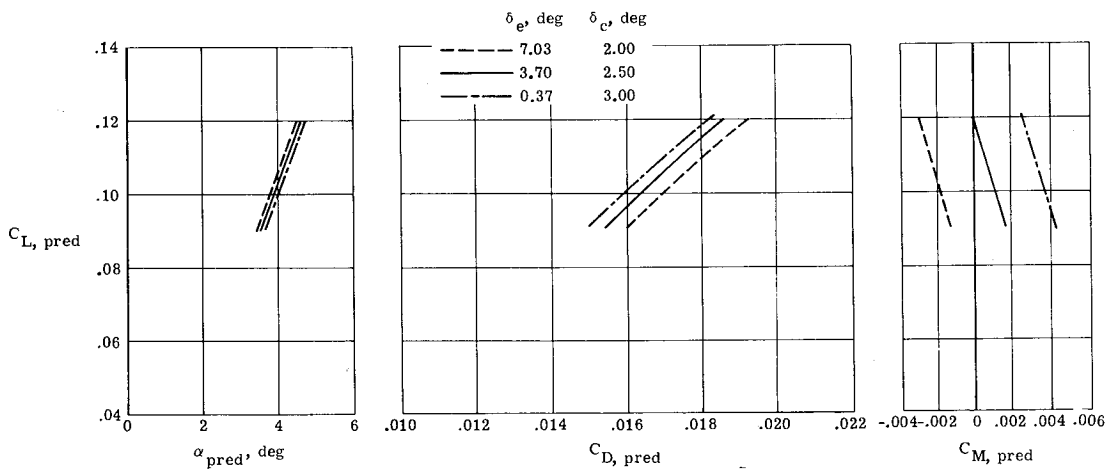
Figure 14.- Continued.



(f) Comparison point P5,  $M_\infty = 1.67$ .

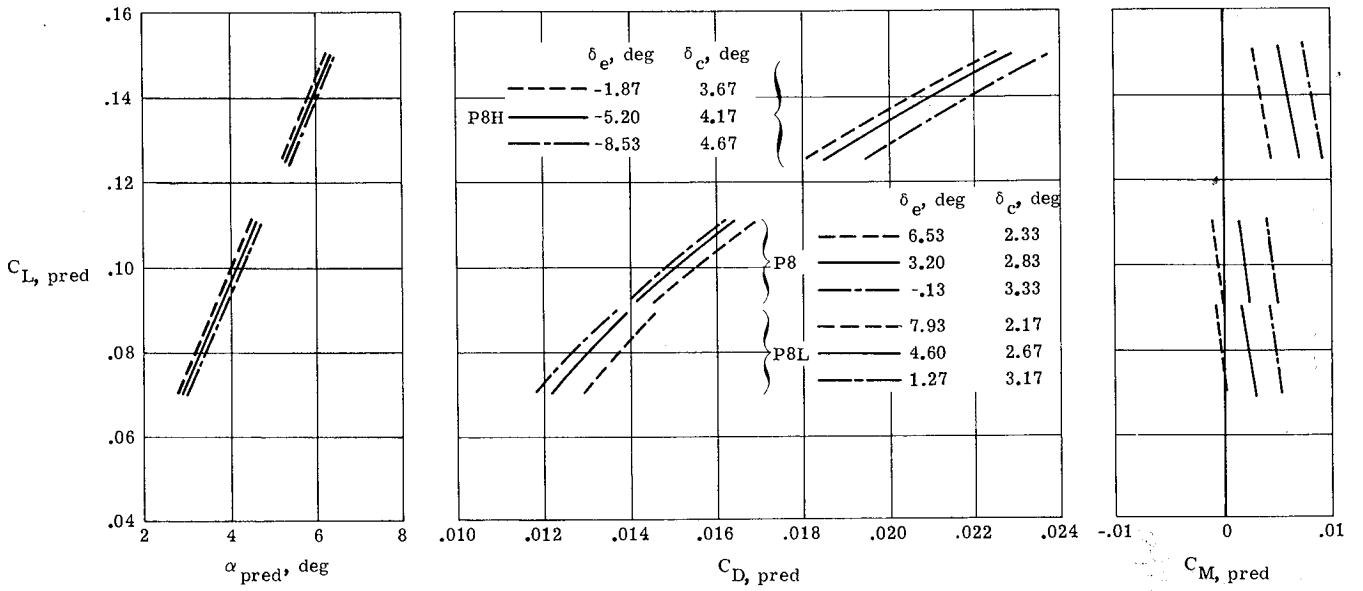


(g) Comparison point P6,  $M_\infty = 2.10$ .

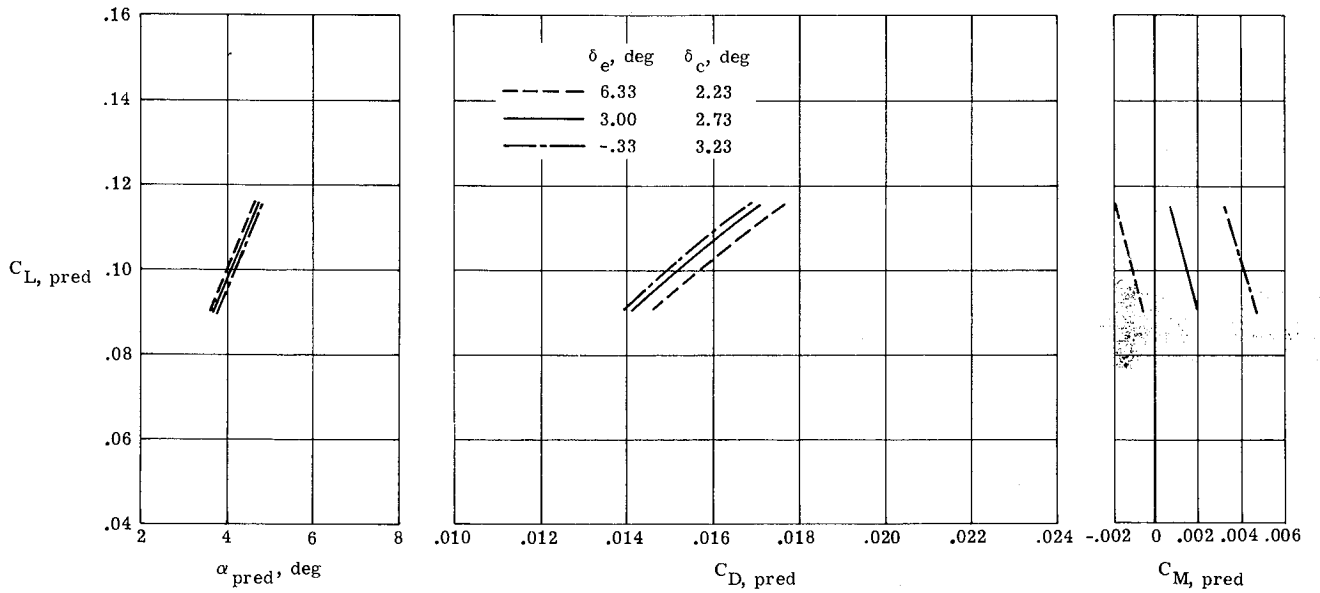


(h) Comparison point P7,  $M_\infty = 2.15$ .

Figure 14.- Continued.

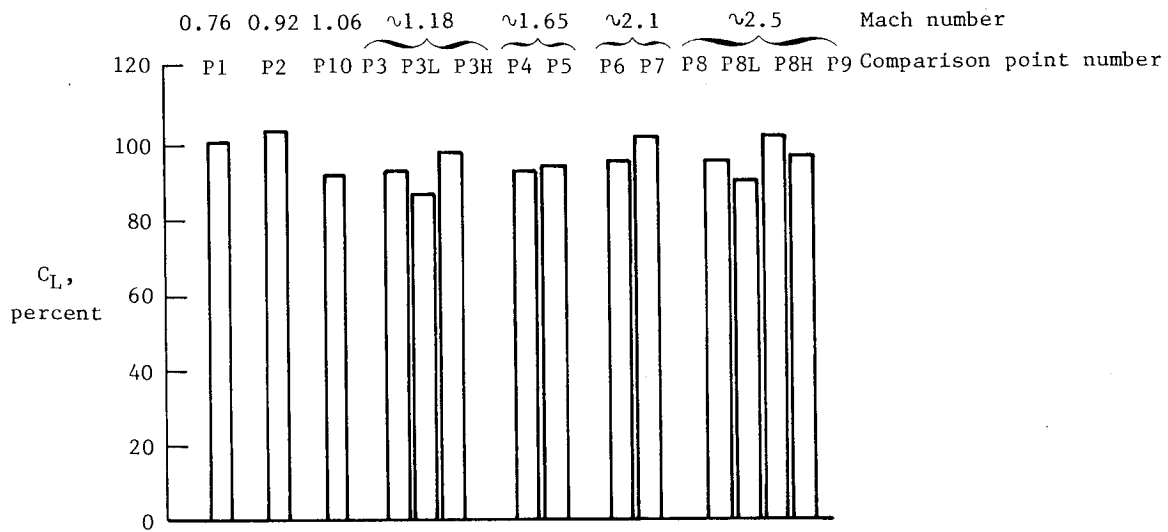


(i) Comparison points P8, P8L, and P8H,  $M_\infty \approx 2.53$ .

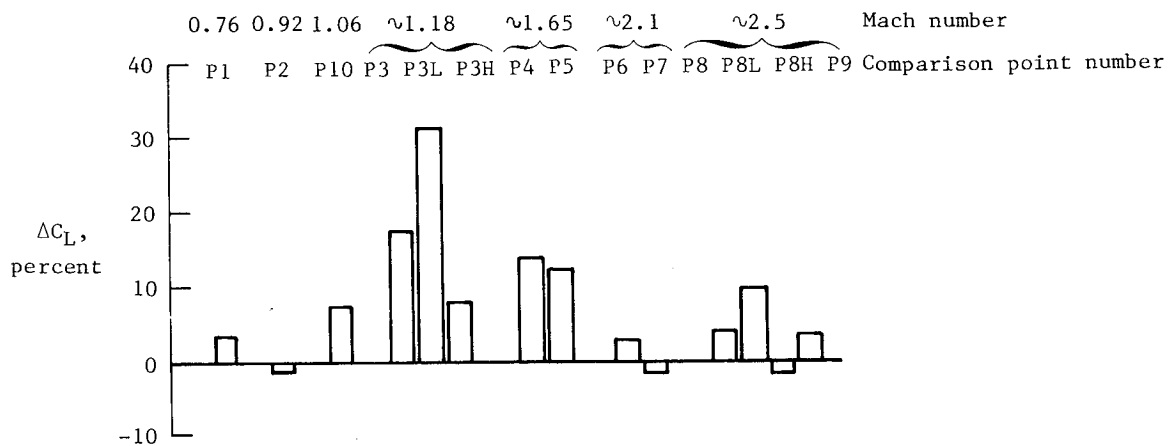


(j) Comparison point P9,  $M_\infty = 2.50$ .

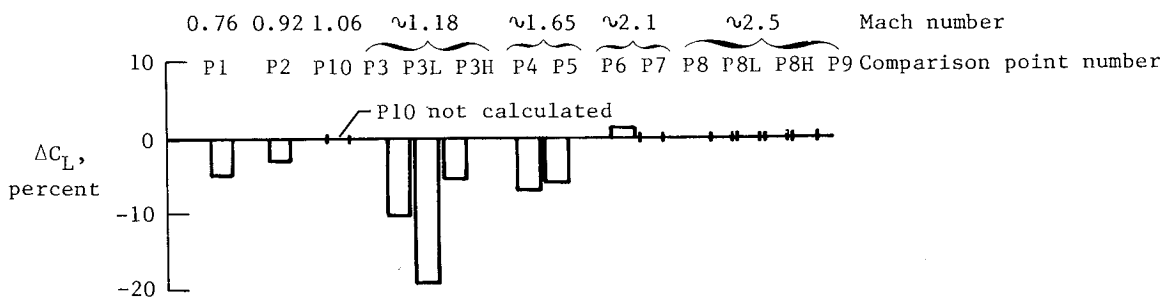
Figure 14.- Concluded.



(a) Wind-tunnel model basic configuration data,  $\delta_e = \delta_c = 0$ .

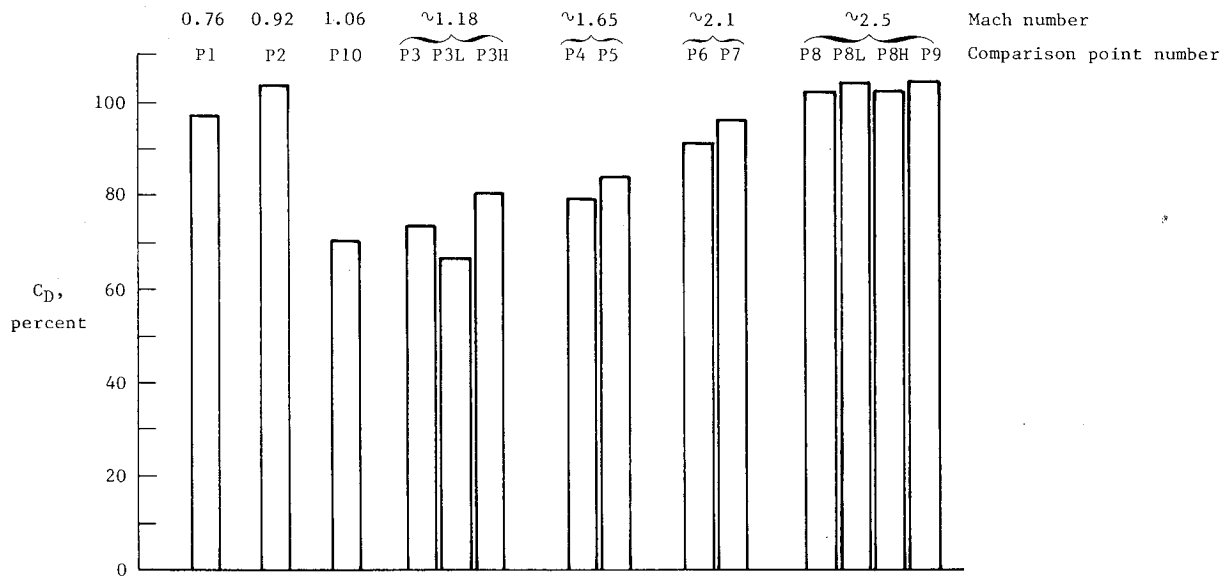


(b) Trim adjustments for  $\delta_e$  and  $\delta_c$ .

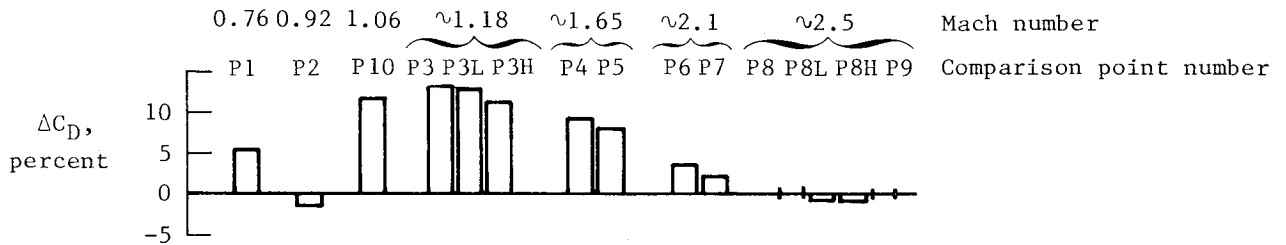


(c) Adjustments for flexibility.

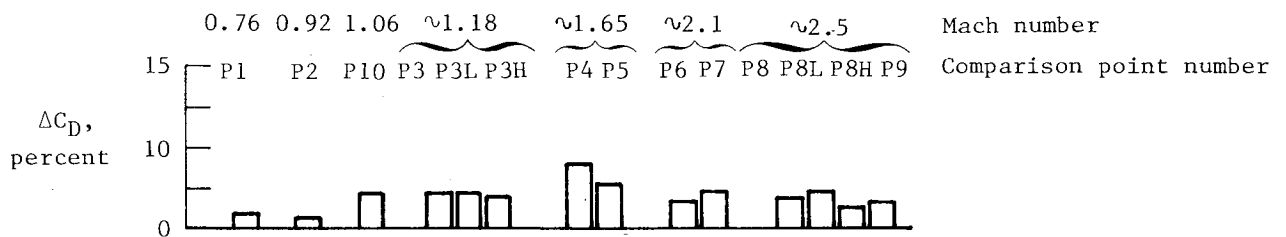
Figure 15.- Percentage of basic wind-tunnel data and adjustments used in prediction for  $C_{L,pred}$  for 14 comparison points.



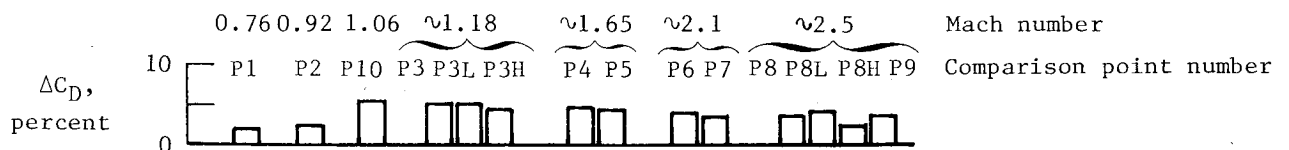
(a) Wind-tunnel model basic configuration data,  $\delta_e = \delta_c = 0$ .



(b) Base drag adjustments.

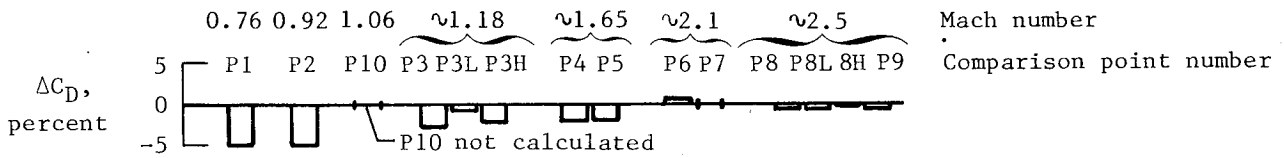


(c) Propulsion system related drag adjustments.

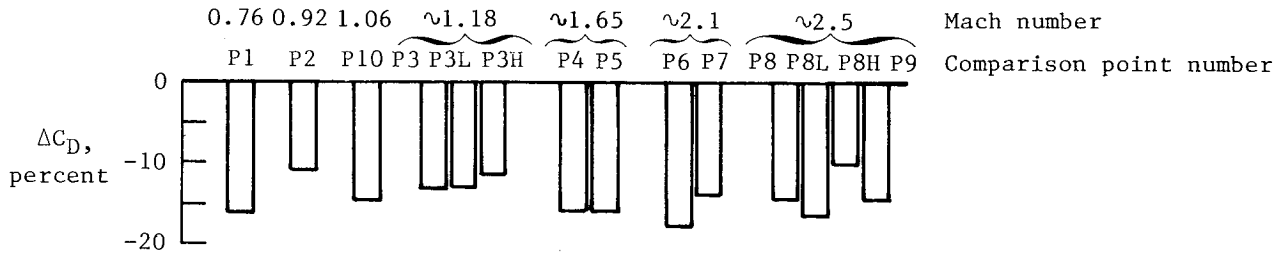


(d) Roughness, protuberance, and air leakage adjustments.

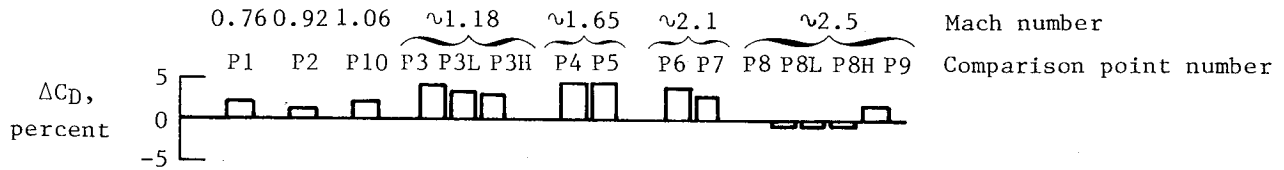
Figure 16.- Percentage of basic wind-tunnel data and adjustments used in prediction for  $C_{D,pred}$  for 14 comparison points.



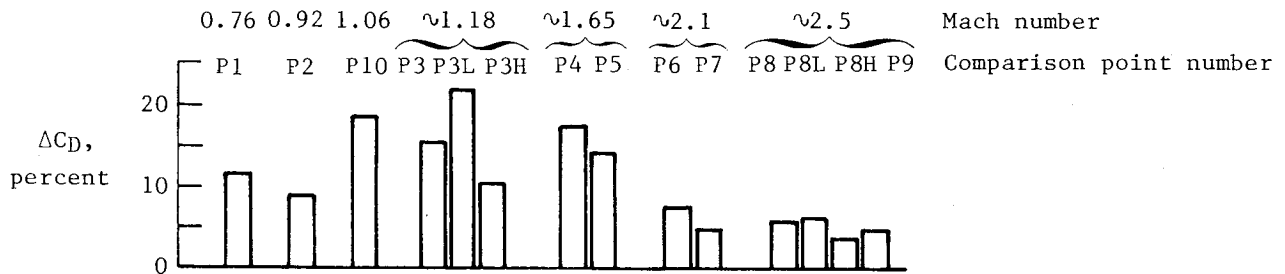
(e) Flexibility adjustments.



(f) Skin-friction drag adjustments.

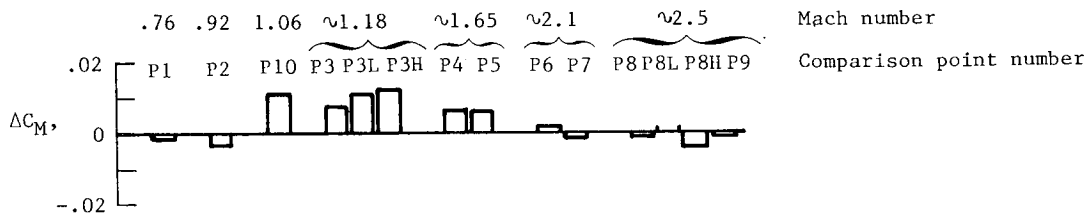


(g) Adjustments for aircraft components not represented on wind-tunnel model.

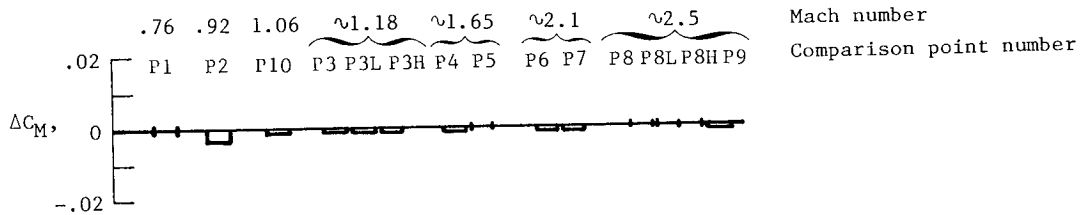


(h) Trim adjustments for  $\delta_e$  and  $\delta_c$ .

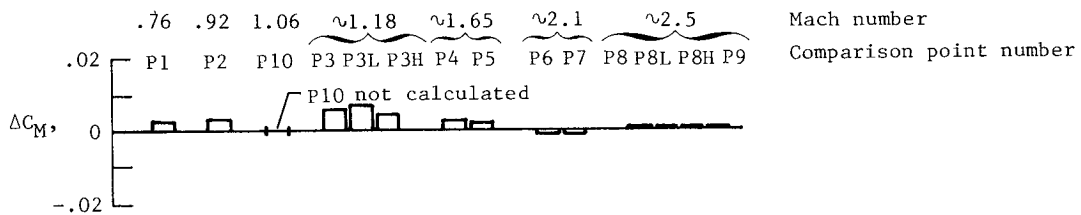
Figure 16.- Concluded.



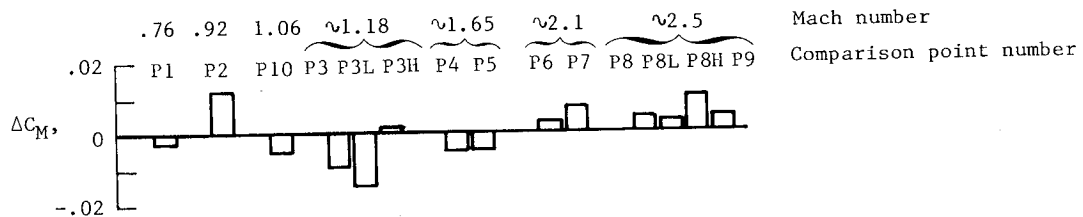
(a) Wind-tunnel model basic configuration data,  $\delta_e = \delta_c = 0$ .



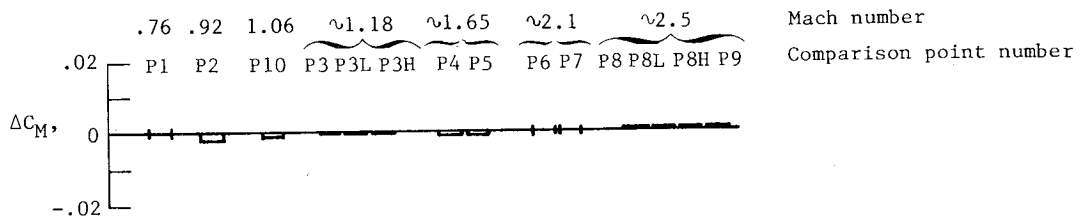
(b) Trim adjustments for  $\delta_e$  and  $\delta_c$  deflections.



(c) Adjustments for airplane components not represented on wind-tunnel model.

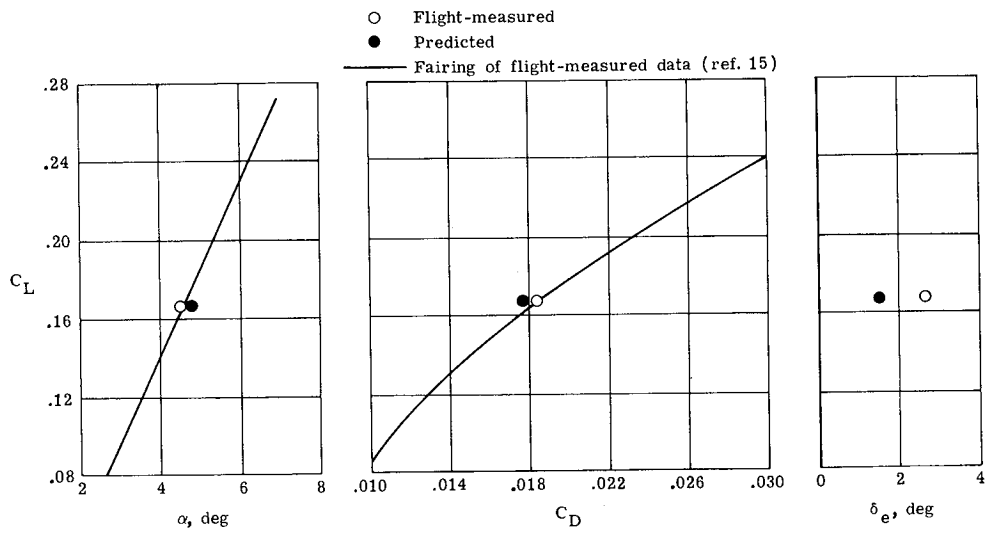


(d) Adjustments for flexibility.

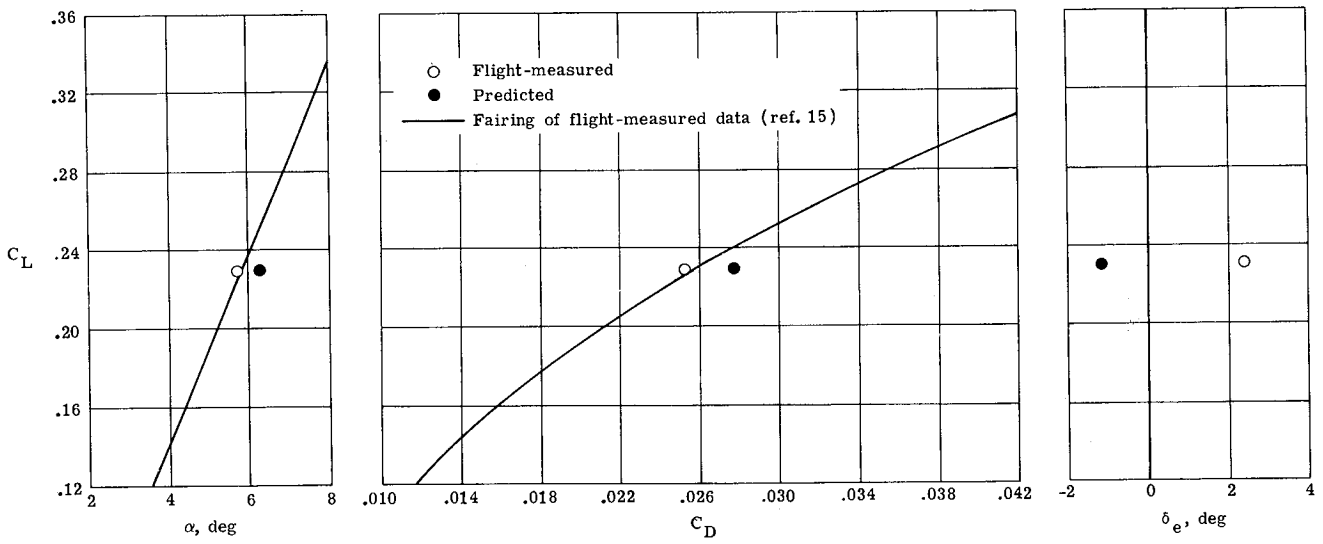


(e) Propulsion system related adjustments.

Figure 17.- Basic wind-tunnel data and adjustments in pitching moment coefficient required to trim predicted data to flight-measured center of gravity.

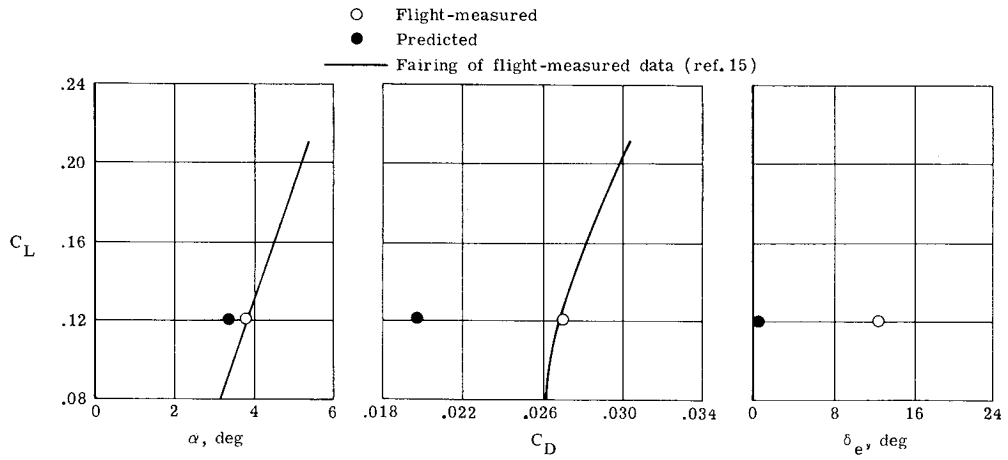


(a) Comparison point P1,  $M_\infty = 0.76$ .

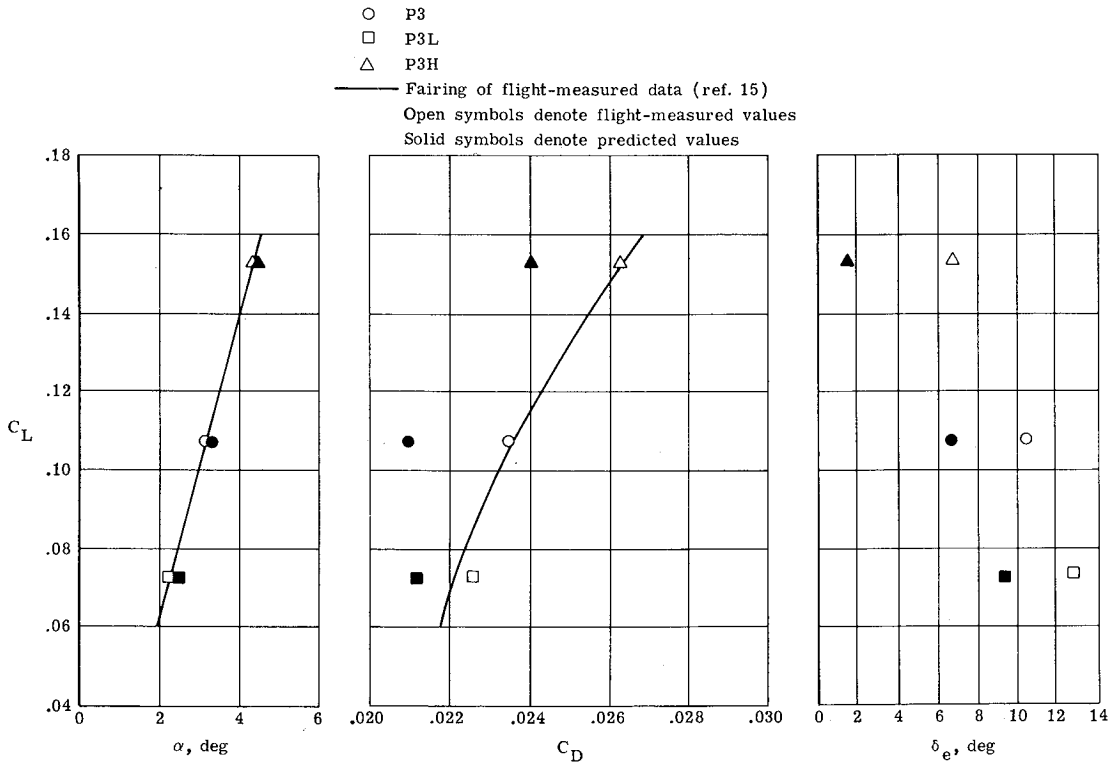


(b) Comparison point P2,  $M_\infty = 0.93$ .

Figure 18.- Predicted and flight-measured aerodynamic characteristics for XB-70-1 airplane for 14 comparison points.

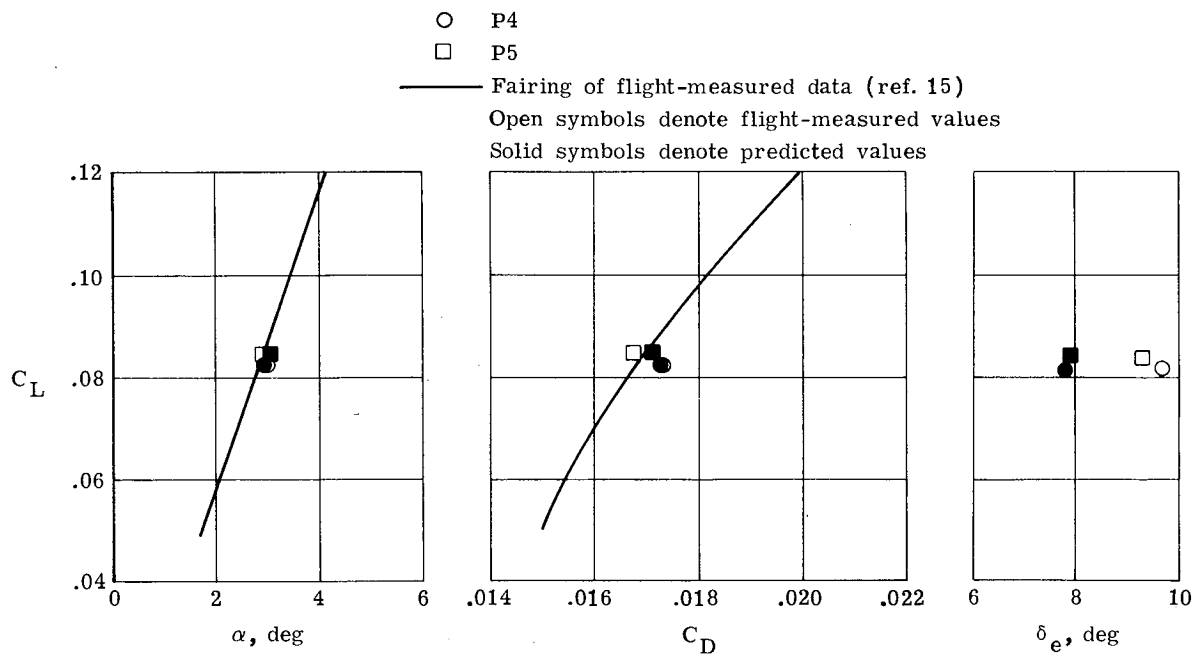


(c) Comparison point P10,  $M_\infty = 1.06$ .

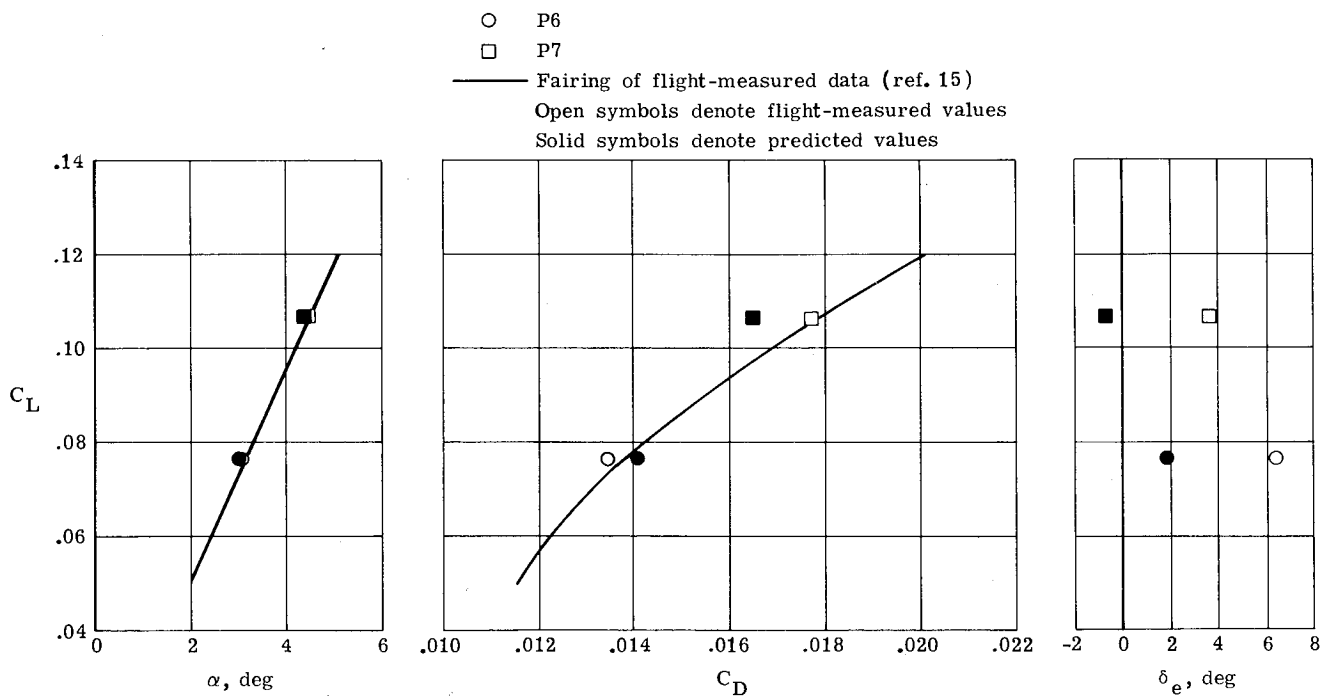


(d) Comparison points P3, P3L, and P3H,  $M_\infty \approx 1.18$ .

Figure 18.- Continued.

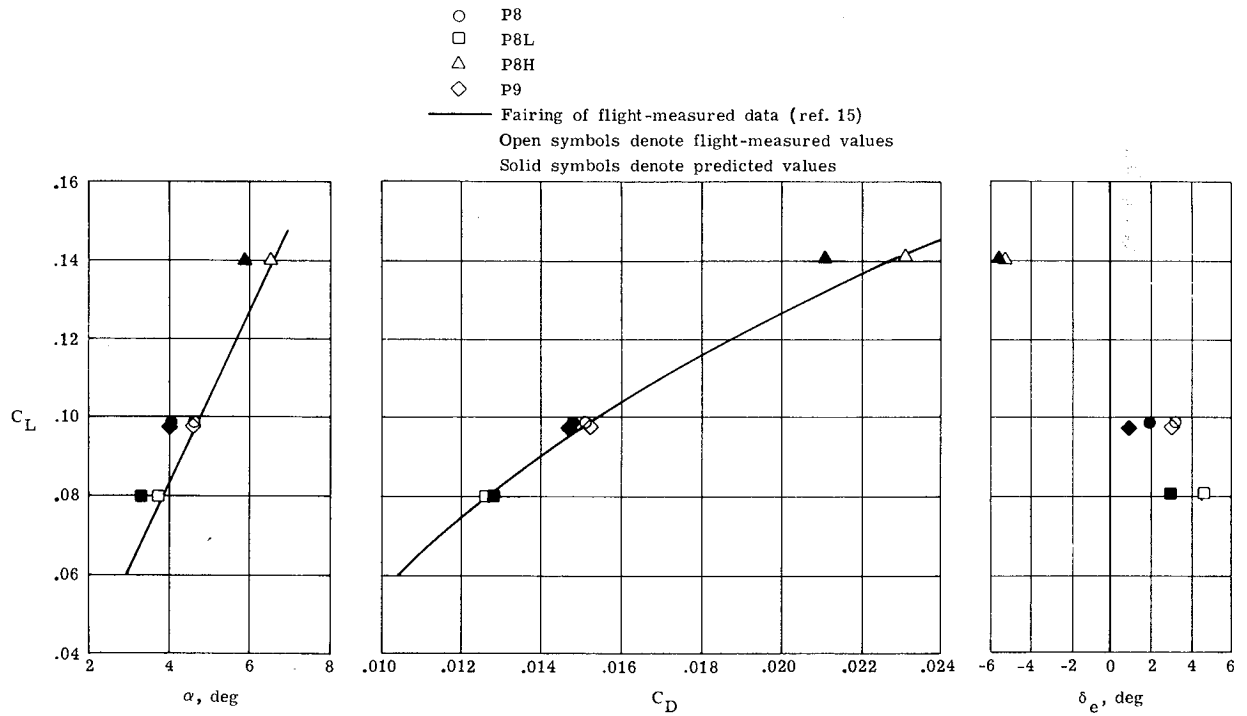


(e) Comparison points P4 and P5,  $M_\infty \approx 1.65$ .



(f) Comparison points P6 and P7,  $M_\infty \approx 2.10$ .

Figure 18.- Continued.



(g) Comparison points P8, P8L, P8H, and P9,  $M_\infty \approx 2.50$ .

Figure 18.- Concluded.

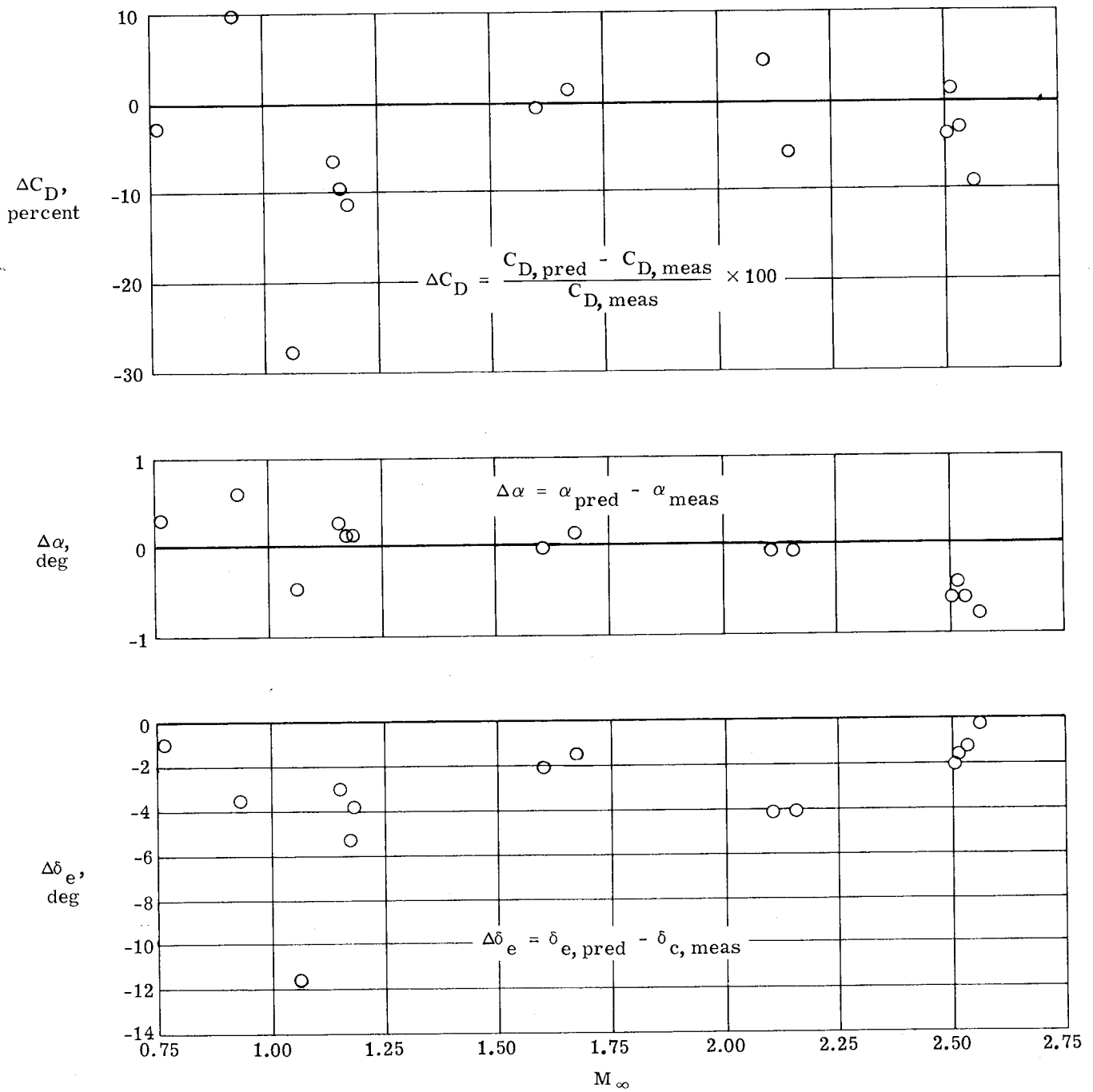


Figure 19.- Summary of the difference between predicted and flight-measured aerodynamic characteristics for 14 comparison points at same  $C_L$  and  $C_M$ .

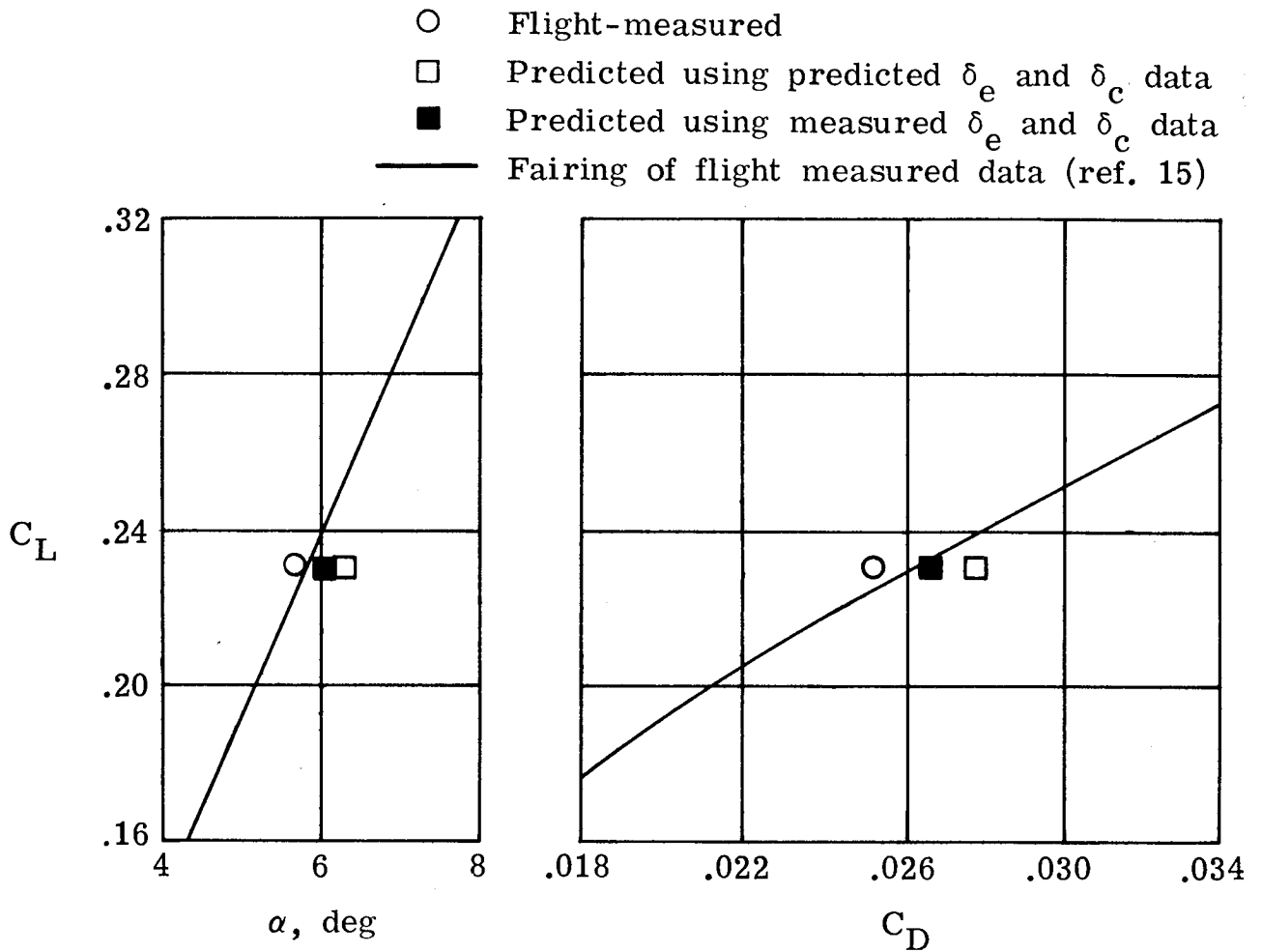


Figure 20.- Comparison of flight-measured values for  $\alpha$  and  $C_D$  with values predicted using  $C_{M,meas}$  or  $\delta_{e,meas}$  and  $\delta_{c,meas}$  for comparison point P2,  $M_\infty = 0.93$ .

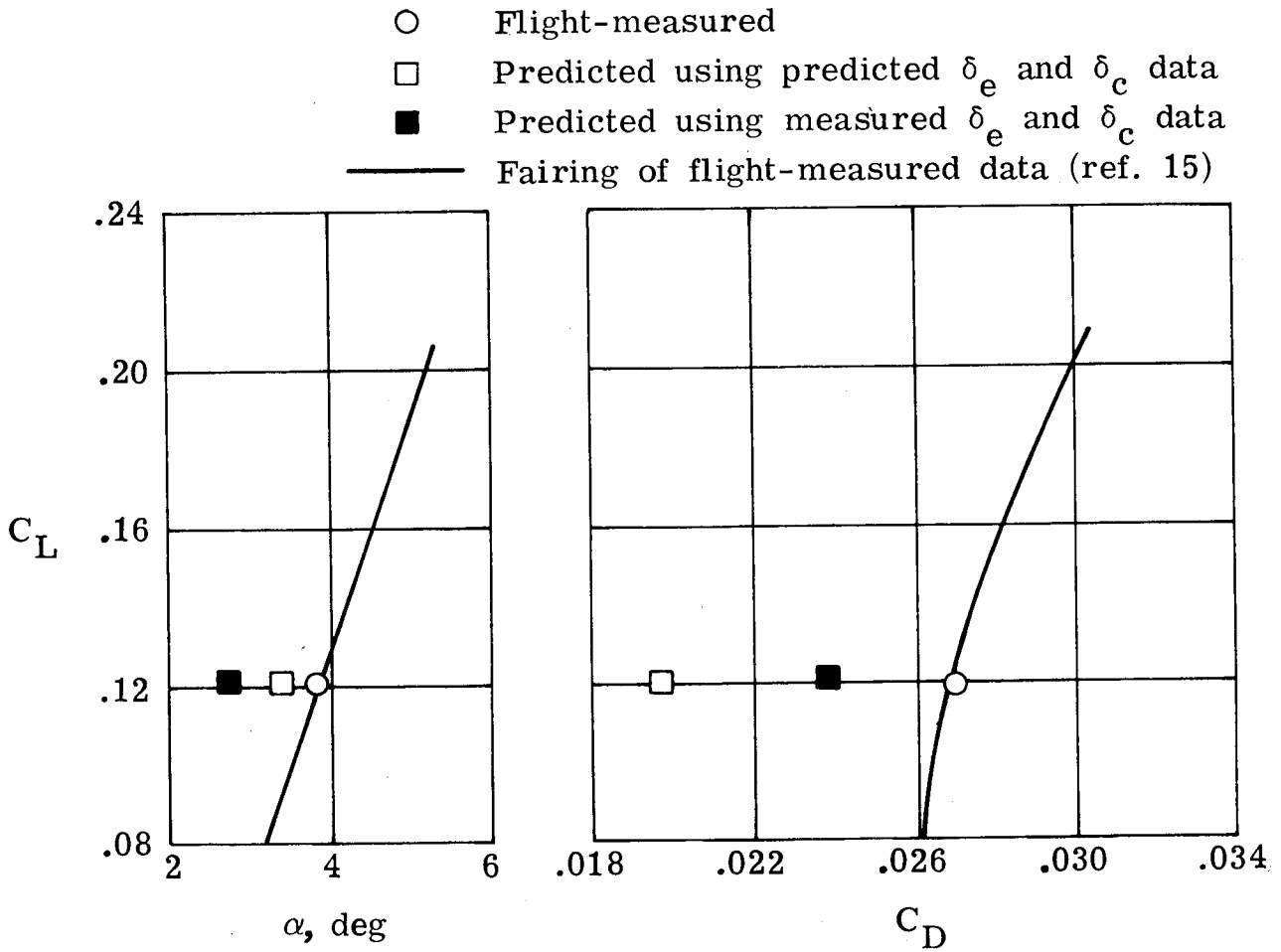


Figure 21.- Comparison of flight-measured values for  $\alpha$  and  $C_D$  with values predicted using  $C_{M,meas}$  or  $\delta_{e,meas}$  and  $\delta_{c,meas}$  for comparison point P10,  $M_\infty = 1.06$ .

- Flight-measured
- Predicted using predicted  $\delta_e$  and  $\delta_c$  data
- Predicted using measured  $\delta_e$  and  $\delta_c$  data
- Fairing of flight-measured data (ref. 15)

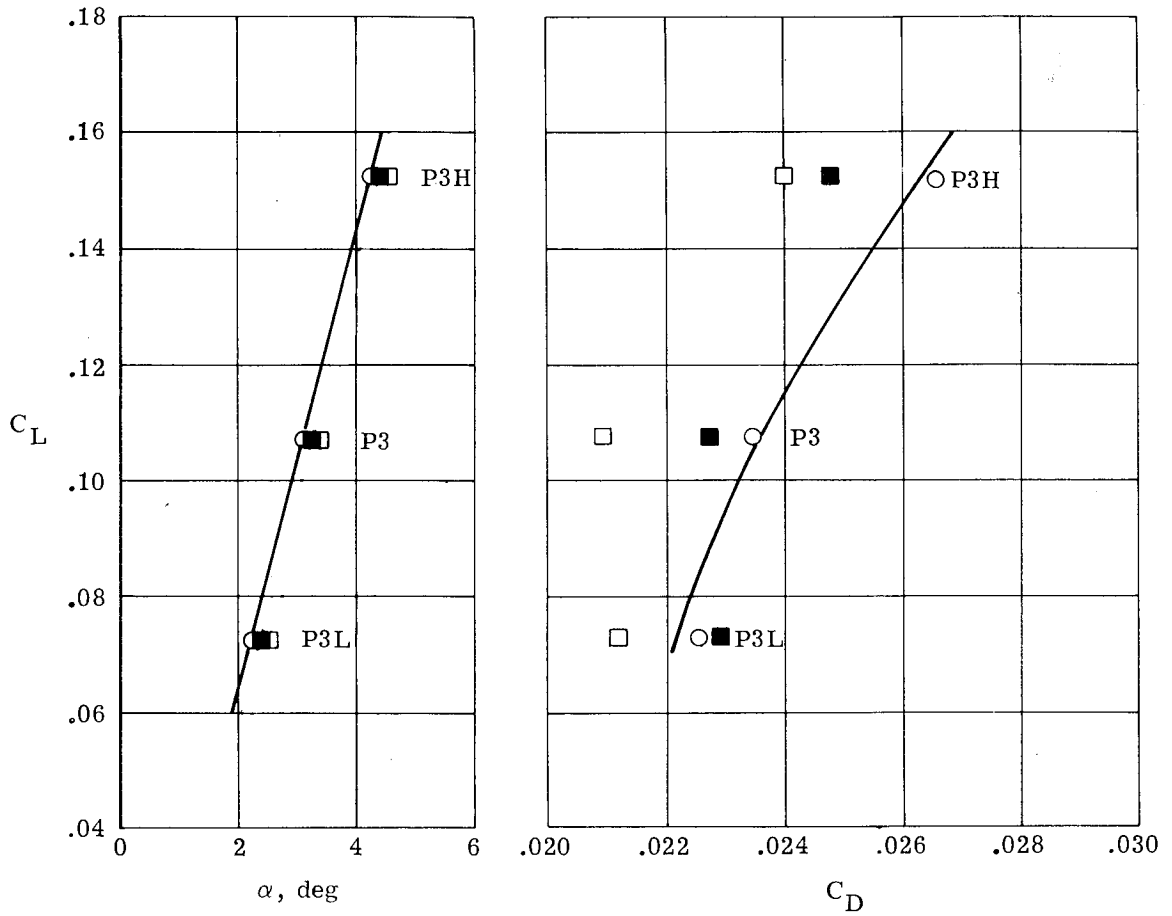
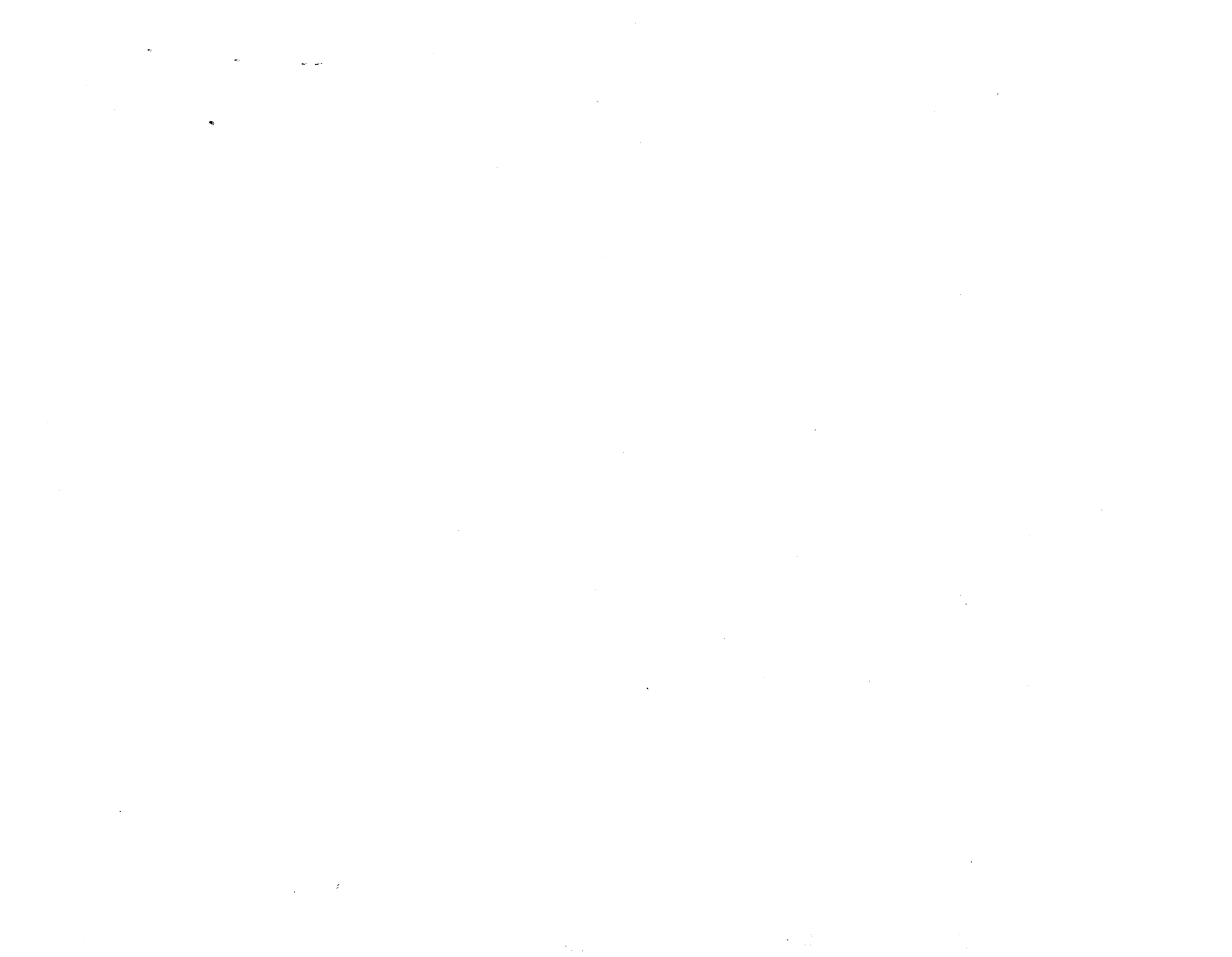


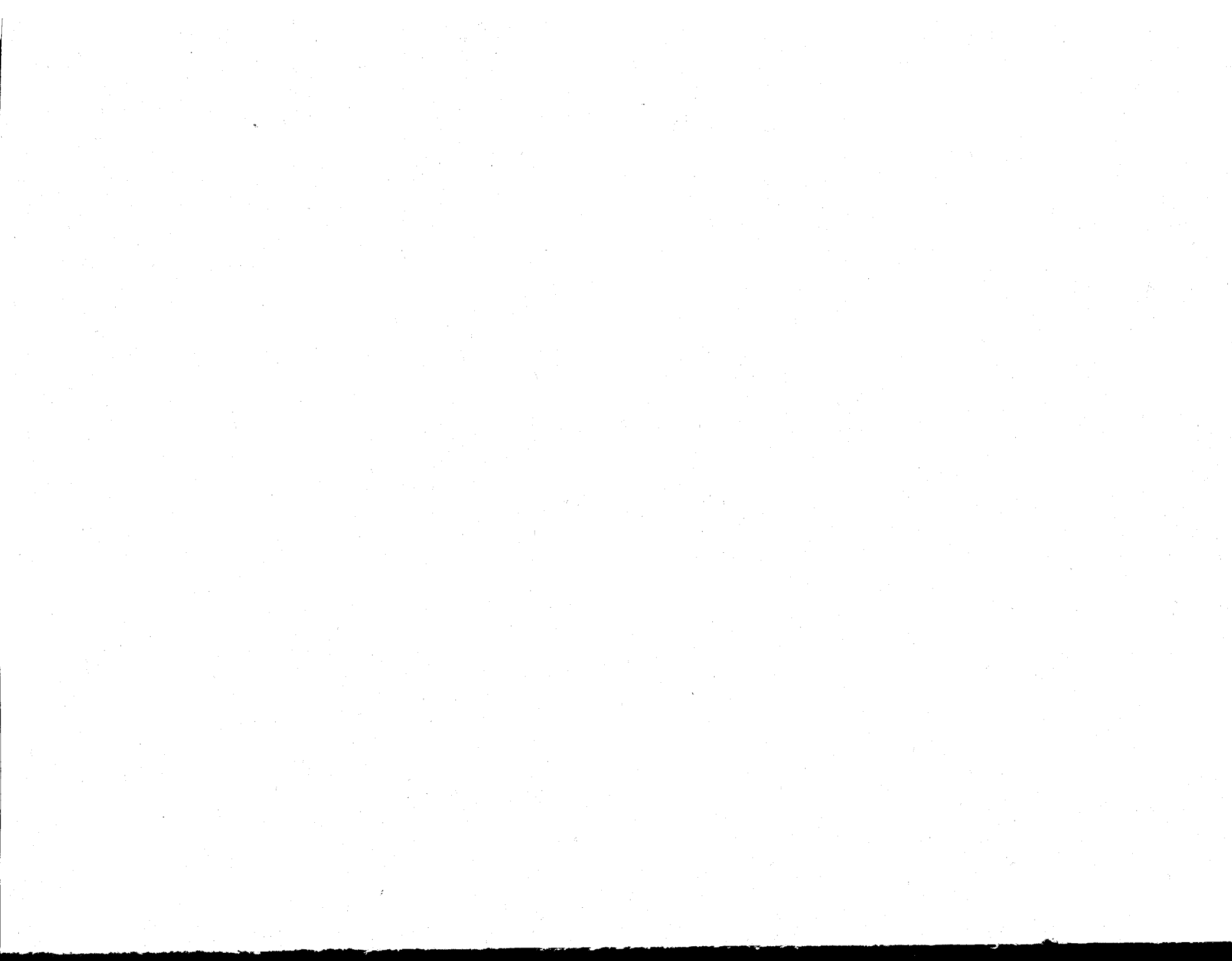
Figure 22.- Comparison of flight-measured values for  $\alpha$  and  $C_D$  with values predicted using  $C_{M,meas}$  or  $\delta_{e,meas}$  and  $\delta_{c,meas}$  for comparison points P3, P3L, and P3H,  $M_\infty \approx 1.18$ .



1. Report No. NASA TP-1516		2. Government Accession No.		3. Recipient's Catalog No.	
4. Title and Subtitle WIND-TUNNEL/FLIGHT CORRELATION STUDY OF AERODYNAMIC CHARACTERISTICS OF A LARGE FLEXIBLE SUPERSONIC CRUISE AIRPLANE (XB-70-1). III - A COMPARISON BETWEEN CHARACTERISTICS PREDICTED FROM WIND-TUNNEL MEASUREMENTS AND THOSE MEASURED IN FLIGHT				5. Report Date March 1980	
				6. Performing Organization Code	
7. Author(s) Henry H. Arnaiz, John B. Peterson, Jr., and James C. Daugherty				8. Performing Organization Report No. H-1079	
9. Performing Organization Name and Address  Dryden Flight Research Center Edwards, CA 93523				10. Work Unit No. 505-43-24-00	
				11. Contract or Grant No.	
12. Sponsoring Agency Name and Address  National Aeronautics and Space Administration Washington, DC 20546				13. Type of Report and Period Covered Technical Paper	
				14. Sponsoring Agency Code	
15. Supplementary Notes  Henry H. Arnaiz: Dryden Flight Research Center, Edwards, California. John B. Peterson, Jr.: Langley Research Center, Hampton, Virginia. James C. Daugherty: Ames Research Center, Moffett Field, California. Part I - NASA TP-1514. Part II - NASA TP-1515.					
16. Abstract  A program was undertaken by the NASA to evaluate the accuracy of a method for predicting the aerodynamic characteristics of large supersonic cruise airplanes. This program compared predicted and flight-measured lift, drag, angle of attack, and control surface deflection for the XB-70-1 airplane for 14 flight conditions with a Mach number range from 0.76 to 2.56. The predictions were derived from the wind-tunnel test data of a 0.03-scale model of the XB-70-1 airplane fabricated to represent the aeroelastically deformed shape at a 2.5 Mach number cruise condition. Corrections for shape variations at the other Mach numbers were included in the prediction. For most cases, differences between predicted and measured values were within the accuracy of the comparison. However, there were significant differences at transonic Mach numbers. At a Mach number of 1.06 differences were as large as 27 percent in the drag coefficients and 12° in the elevator deflections. A brief analysis indicated that a significant part of the difference between drag coefficients was due to the incorrect prediction of the control surface deflection required to trim the airplane.					
17. Key Words (Suggested by Author(s))  Predicted and measured aerodynamic characteristics Wind tunnel to flight correlation Airplane lift and drag Aerodynamics			18. Distribution Statement  Unclassified - Unlimited  Subject Category 02		
19. Security Classif. (of this report) Unclassified		20. Security Classif. (of this page) Unclassified		21. No. of Pages 56	22. Price* \$5.25

\* For sale by the National Technical Information Service, Springfield, Virginia 22161

NASA-Langley, 1980



National Aeronautics and  
Space Administration

THIRD-CLASS BULK RATE

Postage and Fees Paid  
National Aeronautics and  
Space Administration  
NASA-451



Washington, D.C.  
20546

Official Business  
Penalty for Private Use, \$300

**NASA**

POSTMASTER: If Undeliverable (Section 158  
Postal Manual) Do Not Return

---